Journal of
Food Chemistry & Nanotechnology

https://doi.org/10.17756/jfcn.2025-218

Research Article

Open Access

Sequential Bioprocessing of Unripe Banana Flour to Produce Resistant-starch–rich, Low-glycemic Pasta Flour

William Tchabo[1,2*], Spéro Ulrich Koba Edikou[2], Moriken Sangaré[2], Mamadou Lamarana Souare[2], Ibrahima Kaba[2], Robert Patrick Lekane Tchabo[3] and Joseph Dossou[4]

[1]*Department of Food Science and Nutrition, National Advanced School of Agro-Industrial Sciences (ENSAI), University of Ngaoundere, Ngaoundere, Cameroon*

[2]*Department of Technology and Control of Food Products, Higher Institute of Sciences and Veterinary Medicine of Dalaba, Dalaba, Guinea*

[3]*National Advanced School of Engineering, University of Yaoundé I, Yaounde, Cameroon*

[4]*Faculty of Agronomic Sciences, University of Abomey-Calavi, Cotonou, Benin*

***Correspondence to:**
William Tchabo
Department of Food Science and Nutrition,
National Advanced School of Agro-Industrial Sciences (ENSAI),
University of Ngaoundere,
Ngaoundere, Cameroon.

Department of Technology and Control of Food Products,
Higher Institute of Sciences and Veterinary Medicine of Dalaba,
Dalaba, Guinea.
E-mail: williamtchabo@issmvd.edu.gn; william.tchabo@univ-ndere.cm

Received: September 18, 2025
Accepted: December 18, 2025
Published: December 22, 2025

Citation: Tchabo W, Edikou SUK, Sangaré M, Souare ML, Kaba I, et al. 2025. Sequential Bioprocessing of Unripe Banana Flour to Produce Resistant-starch–rich, Low-glycemic Pasta Flour. *J Food Chem Nanotechnol* 11(4): 179-198.

Copyright: © 2025 Tchabo et al. This is an Open Access article distributed under the terms of the Creative Commons Attribution 4.0 International License (CCBY) (http://creativecommons.org/licenses/by/4.0/) which permits commercial use, including reproduction, adaptation, and distribution of the article provided the original author and source are credited.

Published by United Scientific Group

Abstract

Sequential thermal priming, retrogradation, and fermentation were combined to transform unripe banana flour (UBF) into a resistant starch (RS) rich ingredient with reduced glycemic impact suitable for pasta manufacture. Three factors: Box-Behnken design (BBD) assessed thermal priming temperature (TPT) (70 - 90 °C), retrogradation temperature (RT) (12 - 38 °C), and fermentation time (FT) (2 - 12 h), with lactic acid bacteria (LAB) strain (*Lactiplantibacillus plantarum* and *Levilactobacillus brevis*) as a categorical factor. Reduced cubic and strain specific quadratic models showed strong predictive performance ($R^2 \geq 0.92$) for RS, predicted glycemic index (PGI), retrogradation enthalpy (ΔH_r) and breakdown ratio (BR). At the optimum (70 °C, 25 °C, 2 h), *L. brevis* favored nutritional gains, with 44.79% more RS and 8.76% lower PGI, whereas *L. plantarum* improved techno-functional stability, yielding 24.34% higher ΔH_r and 18.06% lower BR. These findings demonstrate that combining thermal structuring and controlled fermentation provides a controllable process strategy for producing low-glycemic pasta flour from unripe banana. The defined unit operations and operating setpoints provide a scalable processing basis while helping to maintain the nutrition and techno-functionality balance required for pasta manufacture.

Keywords

Lactic acid fermentation, Thermal priming, Retrogradation, Resistant starch, Glycemic index

Introduction

The global incidence of type 2 diabetes is escalating rapidly, necessitating the development of dietary strategies that can mitigate postprandial glucose excursions [1]. Concurrently, there has been a substantial rise in consumer demand for gluten-free staple foods [2]. These converging trends have stimulated significant interest in designing starch systems that effectively slow glucose absorption without compromising food functionality [3]. Pasta presents a strategic target for such innovations due to its widespread consumption, ease of preparation, and shelf stability [4].

However, many commercially available gluten-free pastas often rely on refined starches and hydrocolloids, which can lead to higher glycemic responses and reduced nutritional quality [5, 6]. In contrast, food products rich in RS are known to lower glycemia and improve glucose control [7]. Therefore, developing novel flour formulations that genuinely reduce glycemic impact while maintaining desirable processing performance and textural attributes addresses a critical need in functional food development.

Banana is among the most widely cultivated and commercially distributed fruits in tropical and subtropical regions, with year-round availability in local markets across many low and middle-income countries [8]. Its extensive production base, low cost, and well-established value chains make bananas a practical candidate for scalable ingredient development [9]. Moreover, significant postharvest losses frequently occur during periods of peak supply, creating a clear economic and logistical incentive to divert surplus fruit into shelf-stable intermediates such as flour [10]. These factors position bananas, when used as flour, as a locally available raw material with strong potential for incorporation into cereal-type food applications. UBF is particularly promising because its starch is inherently rich in type 2 RS [11]. This type of RS contributes to improved glucose regulation and promotes beneficial colonic fermentation [4]. Despite these nutritional advantages, the unique characteristics of green banana starch pose processing challenges. Its highly crystalline structure resists swelling [12]. Moreover, the absence of gluten limits its functional role in dough, affecting water absorption and weakening dough structure [12]. This often results in increased cooking loss and a soft, crumbly texture in pasta when used at high substitution levels [13]. Consequently, unlocking the full nutritional potential of banana flour in pasta requires targeted modification of its starch matrix.

LAB fermentation is frequently employed to enhance the functional properties of plant flour through dough acidification and enzyme secretion [14]. However, this approach presents a trade-off because the acids and enzymes that enhance dough characteristics can also hydrolyze starch. For instance, prolonged fermentation significantly reduces the peak viscosity of starch pastes [15], potentially consuming native RS and disrupting the starch network [16]. As a result, single-step fermentation often fails to yield flour that is both texturally robust and rich in indigestible starch.

To address this trade-off, the transformation of banana flour should be conceptualized as a sequential engineering process involving a controlled splitting of the starch chain, followed by its reassembly. From a structure process property perspective, maximizing RS content is optimally achieved by inducing retrogradation of starch molecules after gelatinization, cooking, and subsequent cooling [17, 18]. Specifically, long term cooling of gelatinized starch promotes the recrystallization of linear amylose chains into type 3 RS [19]. This approach combines controlled fermentation to generate linear starch fragments with a subsequent programmed cooling step that promotes RS3 formation, thereby compensating for the reduction in indigestible starch caused by fermentation. Additionally, applying a mild thermal pre-treatment modulates starch water-binding capacity and granular organization, enhancing granule susceptibility to targeted hydrolysis while maintaining sufficient structural integrity for dough formation.

The present study seeks to systematically evaluate a sequential bioprocess designed to produce structurally and nutritionally optimized banana-based pasta flour by controlling three critical unit operations, namely TPT, RT, and FT. This processing strategy enables targeted modulation of starch molecular organization while preserving the techno-functional performance required for pasta manufacture. The investigation concentrates on four response variables. RS content serves as the nutritional marker. The PGI reflects the expected postprandial glucose response. ΔH_r represents the degree of molecular reorganization and structural stability. The pasting BR describes mechanical resilience during processing. The overarching objective is to trigger an initial structural disruption and then guide the matrix through a controlled reassembly, enabling the formation of a stable, digestive RS network suitable for pasta production. Given the anticipated nonlinear and interactive nature of the responses, response surface methodology was used to map the multivariate process space. This analytical framework helps identify processing conditions that control starch digestibility and maintain the required techno-functional attributes, thereby providing a basis for developing structurally robust, low-glycemic banana-based pasta. Additionally, two LAB species were compared to ascertain how their differing acidification kinetics and exopolysaccharide (EPS) production influence the flour's structural evolution. To our knowledge, this is the first report to optimize the sequential integration of these unit operations for the production of 100% banana flour suitable for pastification.

Materials and Methods

Materials

Unripe bananas (ripeness stage 2; *Musa sapientum*) were purchased from local agricultural market in Ngaoundere, Cameroon. Analytical grade chemicals and culture media were obtained from Sinopharm Chemical Reagent (China) and Sigma-Aldrich (Germany). *L. plantarum* and *L. brevis* strains were obtained from Dynisco Company (Kunshan, China).

UBF preparation

Unripe bananas were washed, peeled, trimmed, and sliced (~3 mm). Slices were immersed (6 °C, 2 min) in a chilled aqueous mixture containing ascorbic acid (1.0% w/v) and citric acid (0.25% w/v), then drained. The treated slices were dried in a forced-air oven (UF110, Memmert, Germany) at 45 °C for 22 h, arranged in a single layer, until a stable moisture content (8% wet basis) was achieved. The dried slices were subsequently ground using a hammer mill and sieved to obtain particle size ≤ 250 µm. The resulting flour was sterilized following the ultraviolet light-emitting diode method of Du et al. [20], using pulsed 395 nm irradiation. Afterwards, the flour was aseptically packed in airtight, opaque polyethylene bags and stored at 4 °C in the dark until further processing.

Inoculum culture preparation

The LAB inoculum was prepared according to the method described by Kwaw et al. [21], with minor modifications. The LAB species were cultivated in Man, Rogosa, and Sharpe (MRS) broth at 37 °C for 18 h and subsequently subculture twice in fresh MRS broth at 37 °C for 24 h. Following cultivation, the bacterial suspension was centrifuged (Avanti J25, Beckman Coulter, Fullerton, USA) at 3500 rpm for 10 min at 4 °C, and the supernatant was discarded. The resulting cell pellet was washed twice with sterile 0.1% sodium chloride (NaCl) solution. The cell concentration was determined using

a hemocytometer (model XB-K-250, Jianling Medical Device Co., Danyang, China) and adjusted to 10^8 colony-forming unit ml^{-1} with sterile 0.1% NaCl prior to use as the starter culture.

Sequential bioprocessing of UBF for pasta

Thermal priming treatment

The thermal priming treatment was performed using an UBF slurry prepared at a water-to-flour ratio of 3:1 (w/w), under continuous stirring in a circulating water bath (SW22, Julabo GmbH, Germany). Each sample was held for 10 min once the core reached the designated setpoint (±0.2 °C). TPT (X_1) was set at three levels as defined in table 1. No thermal cycling was applied, and priming consisted of a single-step heat exposure. Following thermal priming, all samples were rapidly cooled to under 25 °C to halt thermal progression and ensure consistency prior to the retrogradation step.

Retrogradation treatment

The retrogradation treatment was carried out on the UBF slurry, which was adjusted to a fixed moisture content of 65% (wb). Each sample was vacuum sealed in multilayer pouches and held at 4 °C to stabilize the structure prior to a single annealing step. RT (X_2) was set at three levels as defined in table 1, using a thermostatic circulating water bath (SW22, Julabo GmbH, Germany). Following retrogradation priming at the assigned temperature, the samples were annealed at 55 °C for 60 min and subsequently cooled to 4 °C.

Fermentation treatment

The fermentation treatment was conducted by adjusting the UBF slurry to 18% (w/w) solids. A 3% (v/v) inoculum of actively cultured LAB was incorporated, and the mixture was incubated at 30 °C. FT (X_3) was varied at three levels according to the table 1, using a temperature-controlled incubator (SHP-250, Shanghai Pein Experimental Instrument Co., Ltd, China). At the end of each fermentation period, microbial activity was terminated by heating the slurry at 80 °C for 10 min. The fermented material was then dried at 45 °C to constant weight and milled to pass through a 250 µm sieve.

Experimental design

To investigate the effect of sequential bioprocessing of UBF for producing a high RS pasta flour, a three factor BBD was implemented. The experimental framework was designed to evaluate four independent variables, consisting of three quantitative factors (TPT, RT, and FT) and one categorial factor (strain). The numerical factors TPT (X_1), RT (X_2), and FT (X_3), each coded at three levels, as well as the categorial factor, the strain (X_4) (Table 1), were selected based on preliminary studies. Experimental data from the BBD (Table 2) were analyzed using multiple regression equations and fitted into a reduced cubic model (equation 1):

$$Y = \beta_0 + \beta_s S + \sum_{i=1}^{3} \beta_i X_i + \sum_{i=1}^{3} \beta_{ii} X_i^2 + \sum_{i<j} \beta_{ij} X_i X_j + \sum_{i=1}^{3} \sum_{j=1}^{3} \gamma_{ij} S X_i X_j + \epsilon \quad (1)$$

Where, Y is the predicted response; β_0 is the intercept; S is the strain indicator variable; β_s is the main effect of strain; β_i, β_{ii}, and β_{ij} are the coefficients of the linear, quadratic and two-factor interaction (2FI) terms in the process variables; γ_i and γ_{ij} are the coefficients of the strain × factor and strain × (factor × factor) interaction terms; and ε is the random error term.

When the strain × factor interaction terms were significant in the reduced cubic model, the effects of TPT, RPT, and FT were analyzed separately for each strain to account for strain-specific responses. A quadratic model (equation 2) was fitted individually for *L. plantarum* and *L. brevis*:

$$Y = \beta_0 + \sum_{i=1}^{3} \beta_i X_i + \sum_{i=1}^{3} \beta_{ii} X_i^2 + \sum_{i=1}^{2} \sum_{j=i+1}^{3} \beta_{ij} X_i X_j \quad (2)$$

Where, Y is the predicted response; β_0, β_i, β_{ii}, and β_{ij} are the regression coefficients for the intercept, linear, quadratic and interaction terms, respectively; and X_i and X_j represent the independent numerical variables.

Analytical assays

RS

The RS content was determined based on the procedure described by Khoozani et al. [22], utilizing a Megazyme RS assay kit (Megazyme International Ireland Ltd, Bray, Ireland). UBF samples were incubated with pancreatic α-amylase (A3176, Sigma-Aldrich) and amyloglucosidase (E-AMGDF, Megazyme) in a shaking water bath at 37 °C for 16 h to ensure complete hydrolysis of digestible starch. After enzymatic treatment, the suspension was centrifuged, and the resulting pellet was washed with 50% (v/v) ethanol to eliminate soluble residues. The residual RS was solubilized by vigorous stirring in 2 M potassium hydroxide within an ice water bath for 20 min. This solubilized starch was subsequently hydrolyzed to glucose using amyloglucosidase, and the glucose concentration was measured via a glucose oxidase/peroxidase colorimetric (GOPOD) assay. The RS content was then calculated using a glucose-to-starch conversion factor of 0.9.

Table 1: Coded and actual values of the independent variables in BBD.

Independent variables	Symbols	Coded levels		
	X	-1	0	1
Numerical factor				
TPT	X_1	70	80	90
RT	X_2	12	30	38
FT	X_3	2	7	12
Categorical factor				
Strain	X_4	-	*L. plantarum*	*L. brevis*

PGI

The PGI was determined following the *in vitro* starch hydrolysis procedure described by Giuberti et al. [23]. Briefly, UBF samples were subjected to enzymatic hydrolysis using α-amylase (A3176, Sigma-Aldrich) and amyloglucosidase (E-AMGDF, Megazyme). Each sample was incubated in a shaking water bath at 37 °C for 180 min, after which enzymatic activity was terminated by boiling the reaction mixture for 10 min. The amount of glucose released into the supernatant at specific time intervals was quantified using the GOPOD assay (K-GLUC, Megazyme). Areas under the hydrolysis curves (AUCs) were calculated up to 180 min, and the hydrolysis index (HI) was determined as the ratio of the AUC of each test sample to that of the reference (white bread, containing 723 g starch/kg dry matter, for which HI = 100). The PGI was then estimated using the regression equation 3:

$$PGI = 1.013 \times HI \quad (3)$$

ΔH_r

The ΔH_r was determined using a differential scanning calorimeter (Mettler Toledo, Switzerland) as outlined by Dong et al. [24], with slight modification. Briefly, sample (5 mg) was placed into a sealed aluminum pan and allowed to equilibrate at 25 °C for 4 h. Thermal scanning was performed from 20 to 120 °C at a heating rate of 5 °C/min. The ΔH_r values were obtained from the thermograms using the instrument's data acquisition software.

Rapid visco analyzer (RVA) BR

The BR was determined using an RVA-4800 (Perten Instruments, Hägersten, Sweden) according to the procedure described by Kongolo et al. [25], with minor modifications. Briefly, 3.5 g of sample was dispersed in 25 ml of distilled water. The slurry was agitated at 960 rpm for 10 s and then maintained at 160 rpm. The temperature profile consisted of holding at 50 °C for 1 min, heating from 50 to 95 °C at 12 °C/min, holding at 95 °C for 3 min, cooling from 95 to 50 °C at the same rate, and finally holding at 50 °C for 2 min. Peak and trough viscosities were recorded using Thermocline v4.1 software. The BR was computed using the equation 4:

$$BR = \frac{Peak - Trough}{Peak} \quad (4)$$

Statistical analysis

All experiments and analytical determinations were conducted triplicate, and results are expressed as mean values. Re-

Table 2: BBD and techno-functional properties of UBF.

Runs	Independent variables				Responses			
	TPT (°C)	RT (°C)	FT (h)	Strain	RS (g/100 g ds)	PGI	ΔH_r (J/g ds)	BR
	X_1	X_2	X_3	X_4				
1	90	25	2	*L. brevis*	14.13	51.05	4.71	0.76
2	70	25	2	*L. brevis*	17.43	49.54	6.08	0.71
3	90	12	7	*L. brevis*	11.61	51.88	3.97	0.80
4	80	12	12	*L. brevis*	11.73	51.80	3.83	0.78
5	90	38	7	*L. brevis*	13.74	50.99	4.91	0.75
6	80	38	2	*L. brevis*	15.75	50.40	5.45	0.72
7	80	12	2	*L. brevis*	14.59	50.47	4.97	0.74
8	90	25	2	*L. plantarum*	7.65	57.12	5.76	0.66
9	70	25	12	*L. plantarum*	9.12	57.02	5.89	0.64
10[a]	80	25	7	*L. brevis*	15.73	50.07	5.48	0.73
11	90	25	12	*L. plantarum*	6.88	58.04	5.17	0.67
12[a]	80	25	7	*L. plantarum*	10.91	55.75	7.17	0.63
13	70	25	2	*L. plantarum*	12.64	53.70	7.77	0.61
14	70	12	7	*L. plantarum*	10.84	55.95	7.09	0.64
15	80	38	12	*L. brevis*	12.78	50.98	5.06	0.73
16[a]	80	25	7	*L. plantarum*	11.14	55.43	6.82	0.62
17[a]	80	25	7	*L. brevis*	15.65	50.13	5.38	0.74
18	90	12	7	*L. plantarum*	5.92	58.58	4.52	0.71
19	80	38	2	*L. plantarum*	11.19	55.63	7.29	0.62
20	70	12	7	*L. brevis*	15.71	50.03	5.08	0.74
21	70	38	7	*L. brevis*	15.33	50.23	5.53	0.73
22	80	38	12	*L. plantarum*	8.38	57.40	5.75	0.64
23[a]	80	25	7	*L. plantarum*	10.95	55.27	7.16	0.63
24	90	38	7	*L. plantarum*	7.86	56.97	6.33	0.65
25	70	25	12	*L. brevis*	13.89	50.91	4.80	0.74
26	80	12	2	*L. plantarum*	9.55	56.24	6.20	0.65
27	70	38	7	*L. plantarum*	10.66	55.27	6.65	0.63
28[a]	80	25	7	*L. brevis*	16.38	50.14	5.58	0.73
29	80	12	12	*L. plantarum*	7.30	57.87	5.14	0.68
30	90	25	12	*L. brevis*	12.44	51.42	4.74	0.77

Note: [a] represents central points (used to determine the experimental error).

sponse surface fitting and statistical modelling were performed using Design-Expert® v13 (Stat-Ease Inc., Minneapolis, MN, USA). Differences in the nutritional and techno-functional properties of UBF with *L. plantarum* and *L. brevis* at their respective optimal conditions were evaluated by analysis of variance (ANOVA). Statistical differences ($p < 0.05$) were assessed with Tukey's honestly significant difference in OriginPro 2025 (OriginLab Corp., Northampton, MA, USA).

Results and Discussion

Model fitting for sequential bioprocessing of UBF

The experimental results obtained from the 30 runs, including three center-point replicates per strain (six center runs in total) to estimate pure error, were generated according to the BBD (Table 2). RS ranged from 5.92 to 17.43 g/100 g dry solid (ds), PGI from 49.54 to 58.58, ΔH_r from 3.83 to 7.77 J/g ds, and BR from 0.61 to 0.80. The lowest RS (5.92 g/100 g ds) and highest PGI (58.58) were observed for running 18 (TPT 90 °C, RT 12 °C, FT 7 h, *L. plantarum*). In contrast the highest RS (17.43 g/100 g ds) occurred in run 2 (TPT 70 °C, RT 25 °C, FT 2 h, *L. brevis*). The greatest ΔH_r (7.77 J/g ds) together with the lowest BR (0.61) was recorded in run 13 (TPT 70 °C, RT 25 °C, FT 2 h, *L. plantarum*). These trends indicate that TPT, RT, FT, and strain markedly affected the nutritional and techno-functional properties of UBF. Consequently, the data in table 2 were fitted to several polynomial models (linear, 2FI, quadratic, and reduced-cubic). Model adequacy statistics (Table 3) showed that both the reduced cubic and quadratic models provided highly significant regressions ($p < 0.0001$) for all the responses (RS, PGI, ΔH_r, and BT). For these models, adjusted R^2 as well as predicted R^2 values exceeded 0.941 and 0.875, respectively. The relatively small gaps between adjusted and predicted R^2 (< 0.07), together with non-significant lack of fit for these models ($p > 0.05$), indicate good explanatory and predictive performance [26]. In contrast, the linear and 2FI model exhibited lower adjusted R^2 (< 0.970) and significant lack of fit ($p < 0.05$) for several responses. Although full cubic models yielded slightly higher adjusted R^2 (> 0.985), they were aliased in this BBD. This indicated that certain higher-order effects could not be uniquely estimated and were therefore not interpretable [27]. Therefore, the reduced cubic model was retained as the global model to evaluate the four independent variables (TPT, RT, FT, and strain). When strain × factor interaction terms were significant ($p < 0.05$) in the reduced cubic model, a quadratic model was fitted separately for each LAB species to capture strain-specific effects.

Effects of sequential bioprocessing factors on the properties of UBF

Impact on RS content

TPT exerted a strong and significant effect on RS (Table 4) through both its linear (X_1) and quadratic (X_1^2) terms ($p < 0.0001$). The corresponding negative coefficient estimates (CE), indicate that RS decreases as TPT increases, with the decline becoming more pronounced at the upper end of the temperature range. As stated by Liu et al. [28], a moderate TPT is required to disrupt native RS2 granules and to expose amylose chains that can later recrystallize as RS3. At higher TPT, gelatinization and solubilization intensify, starch chains become increasingly fragmented, and the remaining ordered domains are progressively lost [29]. These structural changes reduce the capacity of starch to reorganize into stable, digestion-resistant crystals, thereby accelerating the decline in RS at high TPT [30]. A complementary pattern was observed for

Table 3: Model adequacy summary.

Source	Model p-value	Lack of fit p-value	Adjusted R^2	Predicted R^2	Remarks
RS					
Linear	<0.0001	0.0096	0.8930	0.8779	-
2FI	0.4021	0.0092	0.8953	0.8827	-
Quadratic	<0.0001	0.4534	0.9896	0.9776	Suggested
Reduced cubic	<0.0001	0.6356	0.9925	0.9751	Recommended
Cubic	0.1091	0.9471	0.9945	0.9906	Aliased
PGI					
Linear	<0.0001	0.0088	0.9593	0.9513	-
2FI	0.0625	0.0143	0.9698	0.9637	-
Quadratic	<0.0001	0.1802	0.9929	0.9856	Suggested
Reduced cubic	<0.0001	0.3020	0.9953	0.9803	Recommended
Cubic	0.2450	0.2102	0.9949	0.9487	Aliased
ΔH_r					
Linear	<0.0001	0.0143	0.7575	0.7102	-
2FI	0.0922	0.0210	0.8107	0.7639	-
Quadratic	<0.0001	0.1620	0.9416	0.8757	Suggested
Reduced cubic	<0.0001	0.8766	0.9850	0.9637	Recommended
Cubic	0.0113	0.9898	0.9856	0.9867	Aliased
BR					
Linear	<0.0001	0.0507	0.9473	0.9370	-
2FI	01879	0.0613	0.9544	0.9394	-
Quadratic	<0.0001	0.7808	0.9926	0.9884	Suggested
Reduced cubic	<0.0001	0.9355	0.9942	0.9880	Recommended
Cubic	0.4123	0.9405	0.9934	0.9880	Aliased

Table 4: Analysis of variance of the reduced cubic model for sequential bioprocessing effects on techno-functional responses.

Source	Degree of freedom (DF)	RS (g/100 g ds)			PGI			ΔH_r (J/g ds)			BR		
		CE	Sum of squares (SS)	p-value	CE	SS	p-value	CE	SS	p-value	CE	SS	p-value
Model	19	13.4600	288.7600	< 0.0001***	52.8000	277.7200	< 0.0001***	6.2700	29.2500	< 0.0001***	0.6800	0.0914	<0.0001***
Linear terms													
X_1 (TPT)	1	-1.5900	40.2900	< 0.0001***	0.8375	11.2200	< 0.0001***	-0.5488	4.8200	< 0.0001***	0.0206	0.0068	<0.0001***
X_2 (RT)	1	0.5275	4.4500	< 0.0001***	-0.3094	1.5300	0.0002**	0.3856	2.3800	< 0.0001***	-0.0169	0.0046	<0.0001***
X_3 (FT)	1	-1.2800	26.0400	< 0.0001***	0.7056	7.9700	< 0.0001***	-0.4906	3.8500	< 0.0001***	0.0113	0.0020	<0.0001***
X_4 (LAB strain)	1	2.4600	36.3100	< 0.0001***	-2.6900	43.2600	< 0.0001***	-0.7850	3.7000	< 0.0001***	0.0533	0.0171	<0.0001***
Two-way interaction terms													
X_1X_2	1	0.5788	2.6800	0.0001***	-0.2525	0.5100	0.0070*	0.3425	0.9385	< 0.0001***	-0.0112	0.0010	<0.0001***
X_1X_3	1	0.5750	2.6400	0.0001***	-0.4250	1.4400	0.0002**	0.3250	0.8450	< 0.0001***	-0.0050	0.0002	0.0080*
X_1X_4	1	0.2819	1.2700	0.0021*	-0.2587	1.0700	0.0006**	0.1538	0.3782	0.0005**	-0.0006	6.25E-06	0.5722
X_2X_3	1	-0.0837	0.0561	0.4079	-0.0762	0.0465	0.3318	0.0337	0.0091	0.4569	-0.0050	0.0002	0.0080*
X_2X_4	1	-0.0325	0.0169	0.6456	0.1119	0.2003	0.0604	0.0019	0.0001	0.9527	0.0006	6.25E-06	0.5722
X_3X_4	1	-0.1069	0.1828	0.1501	-0.2494	0.9950	0.0008**	0.1431	0.3278	0.0009**	0.0000	0.0000	1.0000
Three-way interaction terms													
$X_1X_2X_4$	1	0.0487	0.0190	0.6260	-0.0200	0.0032	0.7945	-0.2200	0.3872	0.0005**	0.0012	0.0000	0.4282
$X_1X_3X_4$	1	-0.1125	0.1012	0.2729	0.1750	0.2450	0.0413*	0.0025	0.0001	0.9554	0.0000	0.0000	1.0000
$X_2X_3X_4$	1	0.0562	0.0253	0.5746	-0.1113	0.0990	0.1676	0.1537	0.1891	0.0055*	-0.0025	0.0001	0.1297
Quadratic terms													
X_1^2	1	-0.8187	4.9500	< 0.0001***	0.3452	0.8800	0.0013*	-0.3006	0.6674	< 0.0001***	0.0131	0.0013	<0.0001***
X_2^2	1	-1.1800	10.3300	< 0.0001***	0.5940	2.6100	< 0.0001***	-0.4544	1.5200	< 0.0001***	0.0131	0.0013	<0.0001***
X_3^2	1	-0.8688	5.5700	< 0.0001***	0.4565	1.5400	0.0002**	-0.3494	0.9014	< 0.0001***	0.0019	0.0000	0.2615
Quadratic–linear (strain-by-quadratic) interaction terms													
$X_1^2X_4$	1	0.2875	0.6104	0.0173*	-0.1019	0.0766	0.2198	0.1244	0.1142	0.0208*	-0.0010	8.01E-06	0.5235
$X_2^2X_4$	1	-0.1088	0.0873	0.3065	-0.1681	0.2087	0.0561	0.0231	0.0039	0.6215	-0.0035	0.0001	0.0484*
$X_3^2X_4$	1	-0.0475	0.0167	0.6480	-0.0831	0.0510	0.3105	0.1281	0.1212	0.0181*	-0.0023	0.0000	0.1765
Residual	10	-	0.7520	-	-	0.4472	-	-	0.1522	-	-	0.0002	-
Lack of fit	6	-	0.4012	0.6356	-	0.3249	0.3020	-	0.0528	0.8766	-	0.0000	0.9355
Standard deviation	-	0.2742	-	-	0.2115	-	-	0.1234	-	-	0.0043	-	-
CV%	-	2.3000	-	-	0.3950	-	-	2.1700	-	-	0.6161	-	-
Adjusted-R^2	-	0.9925	-	-	0.9953	-	-	0.9850	-	-	0.9942	-	-
Predicted-R^2	-	0.9751	-	-	0.9803	-	-	0.9637	-	-	0.9880	-	-
Adequate precision	-	52.5270	-	-	52.1104	-	-	38.7327	-	-	55.4200	-	-

Note: Asterisks (*, **, and ***) indicate 5%, 0.1%, and 0.01% significant levels, respectively.

RT (Table 4), where both the linear (X_2) and quadratic (X_2^2) effects were highly significant ($p < 0.0001$), with a positive CE for X_2 and a negative one for X_2^2. This behavior corresponded to RS increasing from low to intermediate RT values, peaking at mid-range, and then declining at higher RT, which reflects the concave response expected for efficient retrogradation. An intermediate RT provides sufficient molecular mobility for chain rearrangement and favors the formation of stable double helices and crystallites, which is optimal for RS3 formation [31]. At lower RT, mobility is too restricted, while at higher RT crystallization becomes less favorable and RS decreases. Moreover, FT (X_3) followed a similar trend to TPT (Table 4) in its statistical pattern. Both the linear (X_3) and quadratic X_3^2 terms were highly significant ($p < 0.0001$) and their CE were negative, showing that RS declined as FT increased. The decline was steeper at higher FT. Short to intermediate FT can favor RS formation through controlled acidification and limited structural changes [32]. In contrast, prolonged FT exposes starch for longer periods to organic acids and amylolytic activities [33]. Under these conditions, gelatinized and retrograded domains are progressively hydrolyzed, leading to erosion of the resistant fraction [34]. Furthermore, the categorical strain (X_4) also contributed significantly ($p < 0.0001$) to RS behavior (Table 4). The positive CE indicates that *L. brevis* preserved more RS than *L. plantarum* under comparable processing conditions. This higher RS retention is consistent with the milder biochemical environment generated by *L. brevis*, characterized by slower acidification, lower extracellular amylolytic activity and regular EPS production [35]. These EPS increase local viscosity, bind water and can form a partial physical barrier around starch domains [36]. The resulting microenvironment slows the diffusion of acids and enzymes toward gelatinized and retrograded regions, limits chain scission and helps to maintain a larger fraction of starch in digestion resistant structures. In addition to the main effects, the interaction between TPT and strain also significantly ($p < 0.05$) influenced RS (Table 4), with its CE being positive, indicating that the slope of the RS response to TPT differs between the two LAB species. At higher TPT the starch matrix is more completely gelatinized and becomes more accessible. Under these conditions *L. plantarum*, which acidifies more rapidly and generally exhibits stronger amylolytic activity, hydrolyses the opened structure more extensively, leading to a steeper decline in RS [37]. In contrast, *L. brevis* acidifies more slowly and exerts weaker hydrolytic pressure causing RS to decrease more gradually [38]. Consequently, as TPT increases, this difference in biochemical intensity makes the relative advantage of *L. brevis* progressively more pronounced. This pattern is evident in figure 1, where the RS curves for *L. brevis* lie consistently above those for *L. plantarum* over the whole TPT range, and the gap widens at elevated temperatures. Moreover, the negative pure quadratic term X_1^2 produces a pronounced downward curvature in the RS response of *L. plantarum*. In contrast, the positive $X_1^2X_4$ interaction counteracts this effect in *L. brevis*, reducing the curvature and yielding a more stable RS profile. In practical terms, *L. brevis* maintains RS over a wider TPT interval and exhibits a more gradual decline when TPT shifts away the temperature that maximizes RS [39]. In contrast, *L. plantarum* loses RS more sharply under the same thermal stress, consistent with its faster acidification and stronger hydrolytic activity on starch [40, 41]. In parallel with this strain × TPT interaction, the reduced cubic model also identified significant two-way terms between the numeric factors X_1X_2 ($p < 0.001$), X_1X_2 ($p < 0.001$) and X_1X_2 ($p < 0.001$), as shown in table 4. These results confirm that RS formation depends on the combined action of TPT, RT, and FT rather than any single factor. Because strain also had a significant effect ($p < 0.001$), these interactions were re-evaluated with quadratic models separately for *L. plantarum* and *L. brevis*.

The strain-specific models were highly significant, with p values lower than 0.001, adjusted R^2 values above 0.967, coefficients of variation below 2.380, and non-significant lack of fit ($p > 0.05$), indicating strong model adequacy (Table 5 and table 6). Within this framework, the interaction terms X_1X_2 and X_1X_3 remained significant for both strains ($p < 0.05$). The combined effects of TPT and RT on RS (Figure 2a and 2b) show that, at intermediate TPT, increasing RT from low to higher values enhances RS for both strains, whereas high TPT coupled with low RT sharply reduces RS. This pattern suggests that efficient RS3 formation relies on adequate thermal priming of native RS2 followed by cooling that promotes recrystallisation [19]. Moreover, the RS response surface for *L. brevis* (Figure 2b) is more strongly dome shaped and attains higher RS values than that for *L. plantarum* (Figure 2a). This pattern is consistent with the larger CE of X_1X_2 interaction terms and the milder hydrolytic activity of *L. brevis*, which allows retrograded structures to accumulate more effectively [37]. Furthermore, the interaction between TPT and FT (Figure 2c and 2d) shows that RS remains high when both factors are kept in the mid-range, whereas high TPT combined with prolonged FT results in the lowest RS. The positive X_1X_3 CE for both species supports this trend, and their larger magnitude in *L. plantarum* indicates a stronger RS loss when TPT and FT increase simultaneously. The response surface for *L. brevis* lies at a higher RS level and exhibits a broader plateau, indicating a greater capacity to preserve RS under moderately intense processing conditions [35]. In contrast, the steeper gradients observed for *L. plantarum* match its faster acidification and stronger amylolytic activity, which drive more rapid RS depletion as TPT and FT increase [37].

Impact on PGI

TPT exerted a strong effect on PGI (Table 4), with both the linear (X_1, $p < 0.0001$) and quadratic (X_1^2, $p < 0.05$) terms significant and having positive CE. This indicates that PGI rises with TPT, and the trend accelerates at higher temperatures. At elevated TPT, starch granules are more fully gelatinized, native RS2 structures are disrupted, and amylopectin-rich domains become highly accessible to digestive enzymes [29]. This transition from ordered, semi-crystalline regions to amorphous zones increases the fraction of rapidly digestible starch, thereby enhancing the glycemic potential [42]. Moreover, RT significantly influenced PGI (Table 4), with both the linear (X_2, $p < 0.001$) and quadratic (X_2^2, $p < 0.0001$) terms significant, with their CE being negative and positive, respectively. This reveals that PGI decreases as RT rises from low to intermediate levels, reaches a minimum in the mid-range, and then increases at higher RT, reflecting the role of cooling in promoting

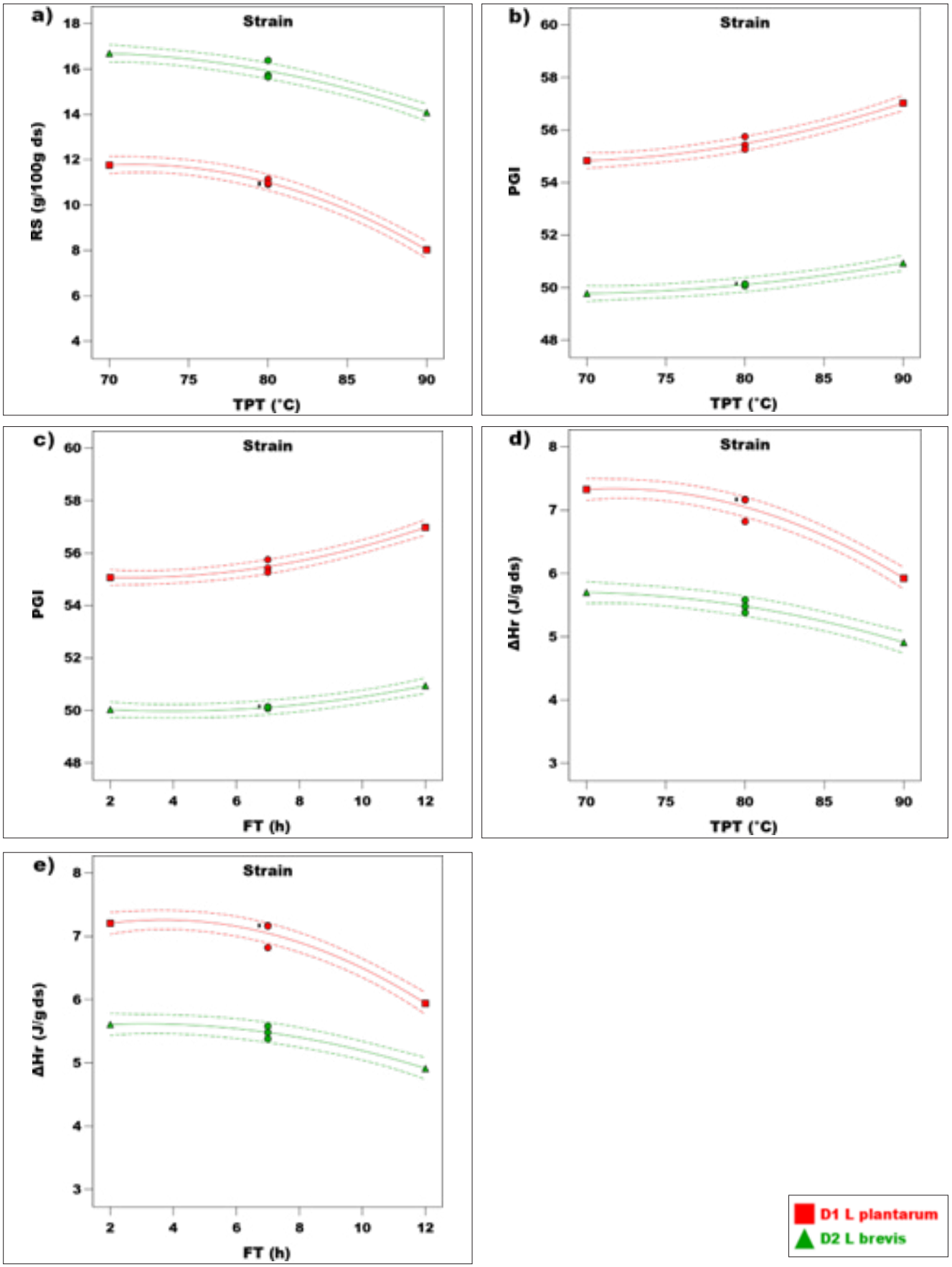

Figure 1: Strain specific reduced cubic response curves showing the combined effects of TPT and FT on the RS, PGI, ΔH_r, and BR of UBF. **(a)** Shows RS as a function of TPT; **(b)** PGI as a function of TPT; **(c)** PGI as a function of FT; **(d)** ΔH_r as a function of TPT; and **(e)** ΔH_r as a function of FT.

Table 5: Analysis of variance of the quadratic model for sequential bioprocessing effects on techno-functional responses of *L. plantarum* fermented UBF.

Source	DF	RS (g/100 g ds)			PGI			ΔH_r (J/g ds)			BR		
		CE	SS	p-value	CE	SS	p-value	CE	SS	p-value	CE	SS	p-value
Model	19	11.0000	54.2700	<0.0001***	55.4800	23.4600	0.0006**	7.0500	12.1200	0.0001**	0.6267	0.0095	0.0002**
Linear terms													
X_1 (TPT)	1	-1.8700	27.9400	<0.0001***	1.1000	9.6100	0.0001**	-0.7025	3.9500	<0.0001***	0.0212	0.0036	<0.0001***
X_2 (RT)	1	0.5600	2.5100	0.0009**	-0.4212	1.4200	0.0081*	0.3837	1.1800	0.0006**	-0.0175	0.0025	<0.0001***
X_3 (FT)	1	-1.1700	10.9300	<0.0001***	0.9550	7.3000	0.0002**	-0.6338	3.2100	<0.0001***	0.0113	0.0010	0.0007**
Two-way interaction terms													
X_1X_2	1	0.5300	1.1200	0.0051*	-0.2325	0.2162	0.1577	0.5625	1.2700	0.0005**	-0.0125	0.0006	0.0021*
X_1X_3	1	0.6875	1.8900	0.0016*	-0.6000	1.4400	0.0078*	0.3225	0.4160	0.0058*	-0.0050	0.0001	0.0668
X_2X_3	1	-0.1400	0.0784	0.2655	0.0350	0.0049	0.8126	-0.1200	0.0576	0.1477	-0.0025	0.0000	0.2956
Quadratic terms													
X_1^2	1	-1.1100	4.5200	0.0002**	0.4471	0.7380	0.0279*	-0.4250	0.6669	0.0021*	0.0142	0.0007	0.0014*
X_2^2	1	-1.0700	4.2600	0.0002**	0.7621	2.1400	0.0034*	-0.4775	0.8419	0.0012*	0.0167	0.0010	0.0007**
X_3^2	1	-0.8213	2.4900	0.0009**	0.5396	1.0800	0.0140*	-0.4775	0.8419	0.0012*	0.0042	0.0001	0.1204
Residual	5	-	0.2495	-	-	0.3922	-	-	0.0983	-	-	0.0001	-
Lack of fit	3	-	0.2193	0.1759	-	0.2727	0.4201	-	0.0189	0.9156	-	0.0000	0.8576
Standard deviation	-	0.2234	-	-	0.2801	-	-	0.1402	-	-	0.0043	-	-
CV%	-	2.3800	-	-	0.4964	-	-	2.2200	-	-	0.6635	-	-
Adjusted-R^2	-	0.9872	-	-	0.9540	-	-	0.9775	-	-	0.9732	-	-
Predicted-R^2	-	0.9344	-	-	0.8058	-	-	0.9606	-	-	0.9425	-	-
Adequate precision	-	38.0275	-	-	20.2198	-	-	28.8867	-	-	28.9614	-	-

Note: Asterisks (*, **, and ***) indicate 5%, 0.1%, and 0.01% significant levels, respectively.

RS3 formation [43]. At intermediate RT, chain mobility and water availability are sufficient to promote the reassociation of amylose and long-chain amylopectin into ordered crystallites, enhancing RS3 formation and thereby lowering PGI [31]. Conversely, low RT, retrogradation is incomplete, whereas at very high RT the thermodynamic driving force for recrystallisation is reduced [44]. In both cases, a larger fraction of starch remains in digestible amorphous domains, resulting in higher PGI relative to the mid-range plateau [42]. Furthermore, FT significantly affected PGI (Table 4), with both linear (X_3, $p < 0.0001$) and quadratic (X_3^2, $p < 0.001$) terms exhibiting positive CE. Short to intermediate FT allows sufficient acidification and microbial metabolism to induce limited chain rearrangement and modest RS3 formation, thereby moderating PGI [42]. However, prolonged fermentation exposes gelatinized and retrograded domains to organic acids and amylolytic activities for longer periods [45]. Under these conditions, both native and retrograded crystallites undergo progressive hydrolysis, yielding dextrin's and low-molecular-weight fragments that are readily digested, while the structural barriers to enzyme diffusion are gradually eroded [15]. These changes increase the proportion of rapidly digestible starch, thereby raising PGI. This is supported by the strong negative correlations observed between PGI and RS ($r = -0.964$ and $r = -0.972$, respectively for *L. plantarum* and *L. brevis*; figure 3a and 3b). In addition, the strain (X_4), significantly modified PGI ($p < 0.0001$, table 4). The negative CE indicates that, under comparable processing conditions, *L. brevis* yields PGI values lower than *L. plantarum*. This trend aligns with the RS behavior, where *L. brevis* preserved a larger resistant fraction across the same design space. Indeed, the fermentation environment with *L. brevis* is less aggressive toward starch, featuring slower acidification, weaker extracellular amylolytic activity, and more consistent EPS production [35]. The resulting EPS matrix increases local viscosity, retains water, and partially shields starch granules and retrograded clusters, slowing acid diffusion and limiting enzymatic access [46]. As a result, a greater proportion of starch remains in slowly digestible or resistant forms, resulting in consistently lower PGI values in flour fermented with *L. brevis*. Beyond the main effects, several interaction terms significantly influenced PGI. The two-way interactions X_1X_2 ($p < 0.05$), X_1X_3 ($p < 0.001$), X_1X_4 ($p < 0.001$), and X_3X_4 ($p < 0.001$) were all significant (Table 4). The negative CE for X_1X_2 and X_1X_3 indicate that the combined effect of TPT with either RT or FT does not simply sum their individual effects. PGI is highest when TPT is elevated and either RT remains

Table 6: Analysis of variance of the quadratic model for sequential bioprocessing effects on techno-functional responses of *L. brevis* fermented UBF.

Source	DF	RS (g/100 g ds)			PGI			ΔH_t (J/g ds)			BR		
		CE	SS	p-value	CE	SS	p-value	CE	SS	p-value	CE	SS	p-value
Model	19	15.9200	42.4600	0.0003**	50.1100	6.5700	0.0001**	5.4800	4.9300	0.0002**	0.7333	0.0079	0.0003**
Linear terms													
X_1 (TPT)	1	-1.3100	13.6200	<0.0001***	0.5787	2.6800	<0.0001***	-0.3950	1.2500	0.0001**	0.0200	0.0032	<0.0001***
X_2 (RT)	1	0.4950	1.9600	0.0069*	-0.1975	0.3121	0.0031*	0.3875	1.2000	0.0001**	-0.0163	0.0021	0.0001**
X_3 (FT)	1	-1.3800	15.2900	<0.0001***	0.4562	1.6700	<0.0001***	-0.3475	0.9661	0.0002**	0.0113	0.0010	0.0007**
Two-way interaction terms													
X_1X_2	1	0.6275	1.5800	0.0108*	-0.2725	0.2970	0.0035*	0.1225	0.0600	0.0647	-0.0100	0.0004	0.0055*
X_1X_3	1	0.4625	0.8556	0.0331*	-0.2500	0.2500	0.0050*	0.3275	0.4290	0.0015*	-0.0050	0.0001	0.0668
X_2X_3	1	-0.0275	0.0030	0.8691	-0.1875	0.1406	0.0159*	0.1875	0.1406	0.0153*	-0.0075	0.0002	0.0172*
Quadratic terms													
X_1^2	1	-0.5312	1.0400	0.0235*	0.2433	0.2186	0.0066*	-0.1762	0.1147	0.0224*	0.0121	0.0005	0.0029*
X_2^2	1	-1.2900	6.1600	0.0005**	0.4258	0.6695	0.0006**	-0.4312	0.6867	0.0005**	0.0096	0.0003	0.0077*
X_3^2	1	-0.9163	3.1000	0.0026*	0.3733	0.5146	0.0010*	-0.2213	0.1807	0.0094*	-0.0004	6.41E-07	0.8590
Residual	5	-	0.5025	-	-	0.0550	-	-	0.0539	-	-	0.0001	-
Lack of fit	3	-	0.1819	0.7822	-	0.0521	0.0772	-	0.0339	0.5016	-	0.0000	0.8576
Standard deviation	-	0.3170	-	-	0.1049	-	-	0.1038	-	-	0.0043	-	-
CV%	-	2.1900	-	-	0.2070	-	-	2.0600	-	-	0.5750	-	-
Adjusted-R^2	-	0.9673	-	-	0.9768	-	-	0.9697	-	-	0.9678	-	-
Predicted-R^2	-	0.9155	-	-	0.8732	-	-	0.8822	-	-	0.9310	-	-
Adequate precision	-	22.9965	-	-	27.8675	-	-	26.5239	-	-	26.4586	-	-

Note: Asterisks (*, **, and ***) indicate 5%, 0.1%, and 0.01% significant levels, respectively.

low or FT is extended, whereas intermediate RT or moderate FT partially counteract the PGI increase induced by high TPT. Moreover, the significant TPT × strain and FT × strain interactions indicate that the slopes of the PGI response to TPT and FT are steeper for *L. plantarum* than for *L. brevis*, as illustrated in figure 1b and 1c. This demonstrates that under harsher TPT and FT conditions, *L. plantarum* rapidly depletes the RS fraction and produces a highly glycemic product. *L. brevis*, in contrast maintains a lower PGI profile even when conditions deviate from those that maximize PGI. These findings highlight the importance of coupling thermal priming with an appropriate cooling step and controlled fermentation to limit glycemic impact. The strain dependence is further evidenced by the significant three-way interaction terms $X_1X_3X_4$ ($p < 0.05$), showing that the combined effect of TPT and FT on PGI depends strongly on the LAB species.

The strain-specific quadratic models were highly significant ($p < 0.001$, table 5 and table 6), with high adjusted R^2 above 0.954, low coefficients of variation below 0.496 and non-significant lack of fit ($p > 0.05$) to capture and explain how TPT, FT, and their interaction influence PGI in a strain-dependent manner. For both *L. plantarum* and *L. brevis*, the significant X_1X_3 ($p < 0.001$) has a negative CE, indicating that their combined effect on PGI is less than additive. The PGI response surfaces (Figure 4a and 4b) displayed an upward-opening paraboloid, with PGI lowest at intermediate TPT and FT, while PGI increased again as either factor moved toward its lower or upper limit. As reported by Chakraborty et al. [44], high TPT disrupts starch granules and crystalline structures, exposing the matrix to microbial amylases and organic acids during fermentation. This promotes depolymerization of starch chains and the formation of rapidly digestible dextrin's. At lower TPT, starch granules remain partially intact, making FT the main driver of structural relaxation causing a sharp increase in PGI as FT increases. In contrast, at high TPT much of the granular and crystalline structure has already been disrupted [29, 44], so additional FT produces smaller increases in PGI. The negative X_1X_3 coefficient therefore reflected overlapping effects TPT and FT, making their combined impact antagonistic rather than strictly additive. The curvature (Figure 4a and 4b) was steeper for *L. plantarum*

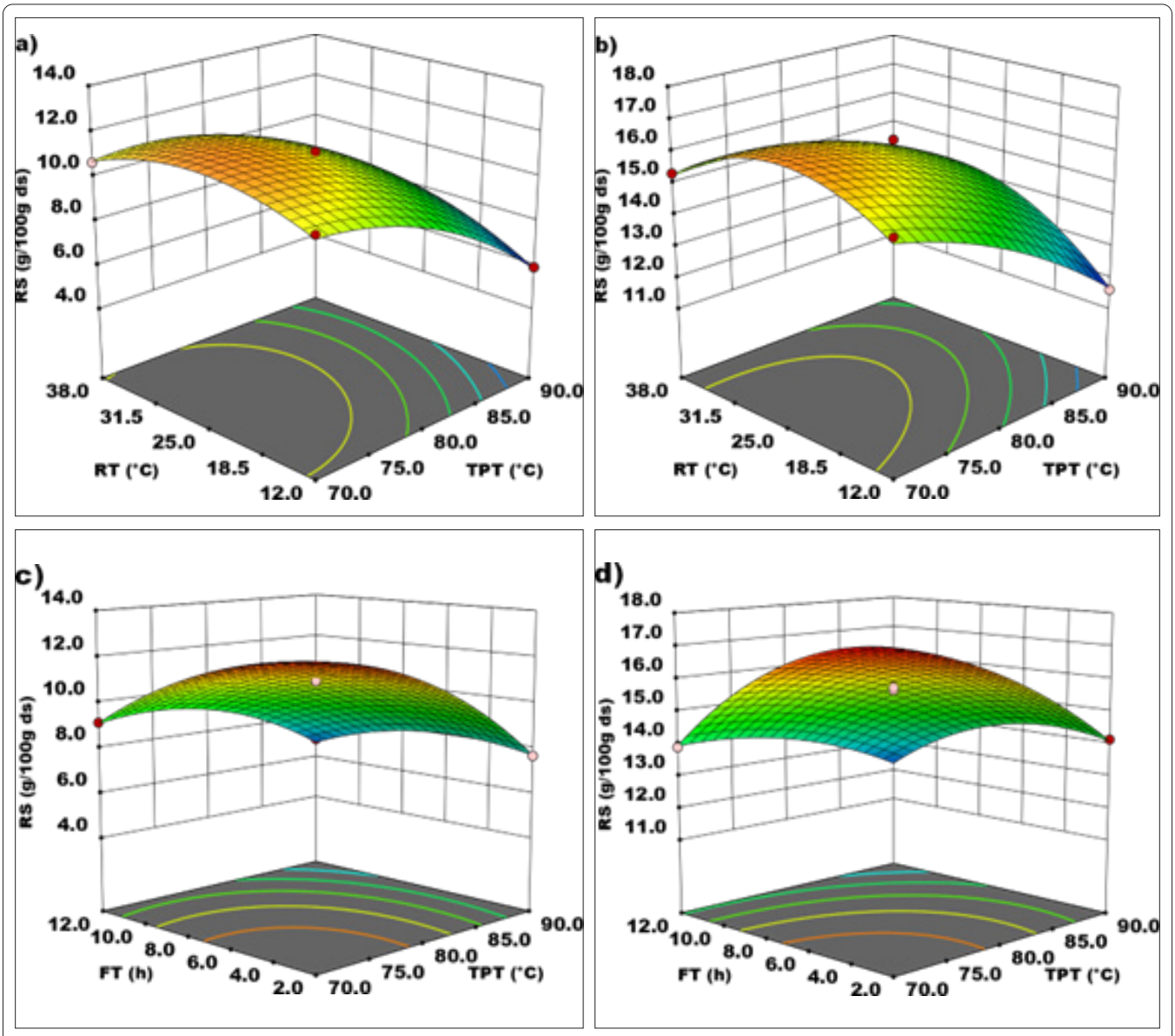

Figure 2: Quadratic response surfaces showing the combined effects of TPT, RT, and FT on the RS content of UBF. **(a, c)** Correspond to *L. plantarum*, and **(b, d)** to *L. brevis*.

than for *L. brevis*, consistent with the more negative X_1X_3 coefficient in the *L. plantarum* quadratic model, that might be attributed to its higher acidification and hydrolytic activity. Besides, the X_2X_3 interaction was significant only for *L. brevis* ($p < 0.05$, table 6). The negative CE indicates that PGI increased more steeply with FT when RT was low, but this slope was attenuated at higher RT (Figure 4c). Intermediate to high RT promotes RS3 formation, as amylose and long-chain amylopectin reassociate into compact double helices and crystallites during cooling [18, 43]. These retrograded domains are less permeable to acids and enzymes [19]. During prolonged fermentation, *L. brevis* continued to erode this network, but the additional PGI increase was smaller at high RT because a substantial fraction of starch remained locked in ordered aggregates, indicating that RT partially buffered the effect of extended fermentation. This behavior is also reflected in the response surface plot for *L. brevis* (Figure 4c), which exhibits an elliptic paraboloid shape. PGI reached its minimum at intermediate FT values and increased at both short and long FT, with the increase at long FT particularly pronounced at high RT. High RT generated a larger pool of well-organized RS3 structures, initially preserved due to the slower acidification and milder amylolytic activity of *L. brevis* [39, 47]. During extended fermentation, these RS3 structures were progressively solubilized, increasing the pool of digestible starch and consequently raising PGI. A further contrast emerged for the X_1X_2 interaction, which was only significant for *L. brevis* ($p < 0.05$, table 6), likely because its slower acidification and milder amylolytic activity make PGI more sensitive to the combined effects of TPT and RT. This sensitivity is reflected in the response surface plot for *L. brevis* (Figure 4e), which exhibited an elliptical paraboloid shape. PGI reached its minimum at intermediate TPT × RT combinations and increased toward both lower and higher extremes, indicating that deviations from optimal thermal conditions reduce RS3 preservation and increase digestible starch, thereby raising PGI. This pattern illustrates the compensatory behavior captured by the negative CE, where high TPT alone elevates PGI by extensively

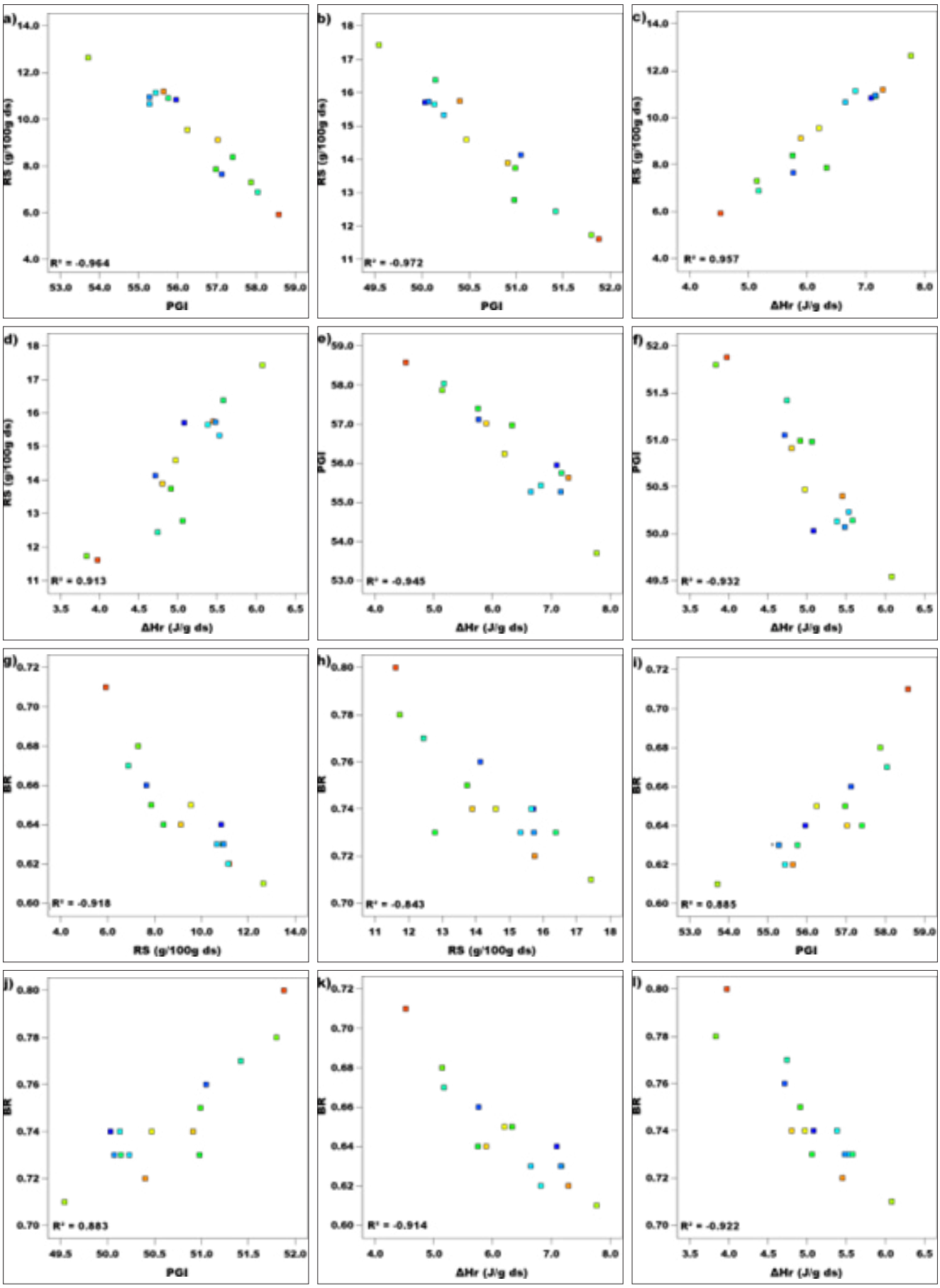

Figure 3: Pairwise relationships between RS, PGI, ΔH_r, and BR for UBF. **(a, b)** Show RS vs PGI, **(c, d)** RS vs ΔH_r, **(e, f)** PGI vs ΔH_r, **(g, h)** BR vs RS, **(i, j)** BR vs PGI, and **(k, l)** BR vs ΔH_r for *L. plantarum* and *L. brevis*, respectively.

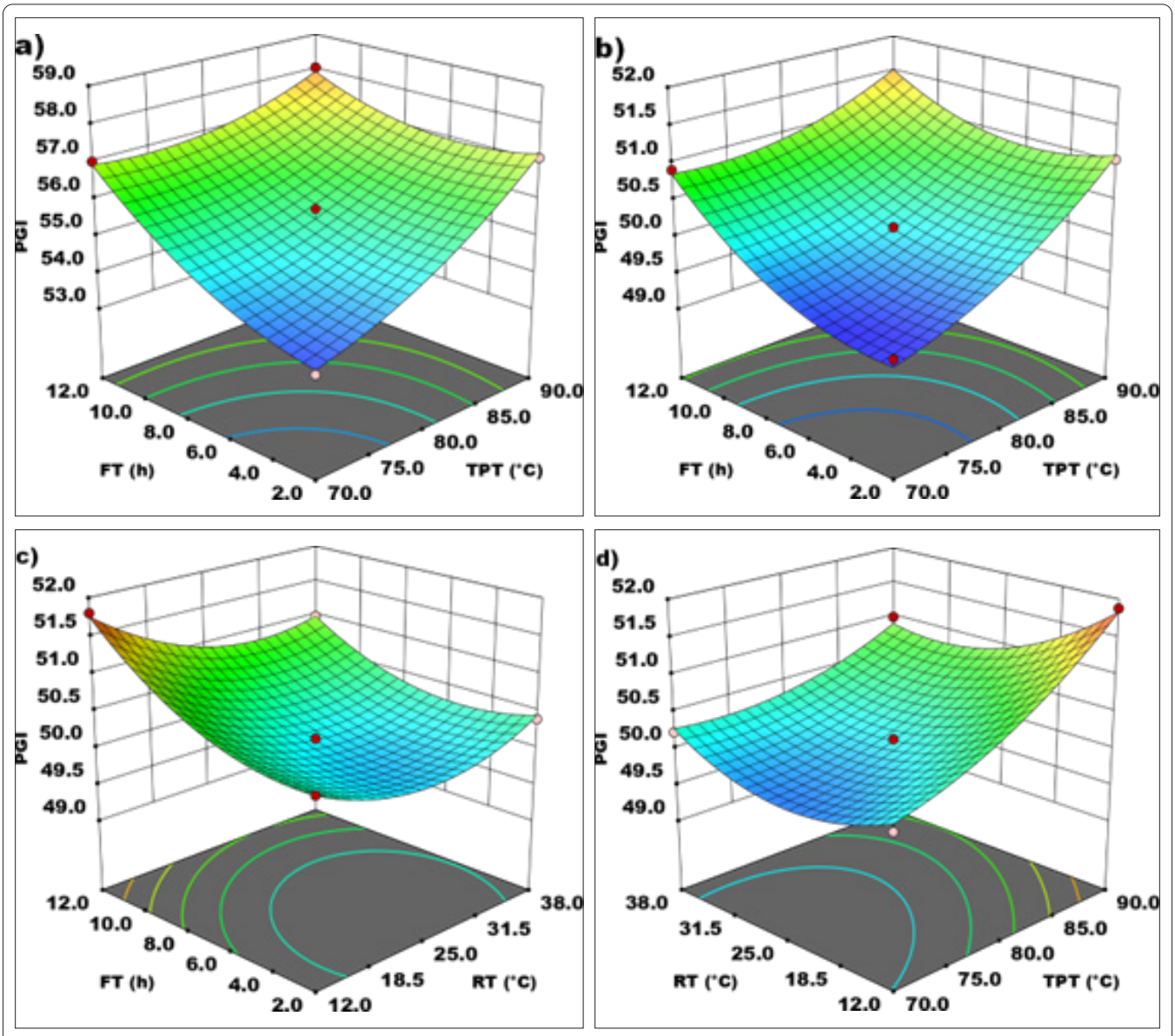

Figure 4: Quadratic response surfaces showing the combined effects of TPT, RT, and FT on the PGI of UBF. **(a)** Correspond to *L. plantarum*, and **(b-d)** to *L. brevis*.

gelatinizing starch, disrupting native RS2, and exposing amylopectin-rich domains to digestion [29, 44]. When RT was raised after strong thermal priming, liberated amylose chains retrograded efficiently to form ordered crystallites [18, 43]. Under the comparatively mild biochemical conditions of *L. brevis*, including slower acidification, lower amylolytic activity, and EPS production, these retrograded amylose-rich crystallites persisted during fermentation [48, 49], limiting the rise in PGI.

Impact on ΔH_r

The experimental results showed that ΔH_r, which reflects starch recrystallization, is highly sensitive to the three quantitative processing variables (Table 4), namely TPT (X_1), RT (X_2), and FT (X_3). Strong linear and quadratic effects were observed for all three factors, each strongly significant ($p < 0.0001$). This pattern points to distinct molecular mechanisms that govern starch behavior during processing. Both TPT and FT exerted a consistently negative effect on ΔH_r. This trend agrees with the expected response of gelatinized starch [44, 50]. The negative CE for both the linear (X_1; X_3) and the quadratic (X_1^2; X_3^2) terms of TPT and FT show that ΔH_r decreases steadily as priming intensity and fermentation duration increase. The decline becomes sharper at the upper end of both factor ranges. This pattern reflects the progressive structural degradation of the starch substrate. As TPT rises, native RS2 granules are disrupted and intense gelatinization occurs [51]. Molecular fragmentation becomes more pronounced, and high thermal loads cause extensive disentanglement of amylose and amylopectin chains [29]. The resulting shorter chains have a reduced capacity to reorganize into extended and stable double helices during cooling [17]. As a result, the formation of well-ordered crystallites that dissipate energy is limited and ΔH_r decreases. The large negative coefficients for X_1 and X_3 indicate that both thermal exposure and FT strongly restrict recrystallisation, with TPT exerting a slightly stronger effect. As FT increases, exposure to microbial amylases and organic acids [45], promoting enzymatic hydrolysis and acid catalyzed

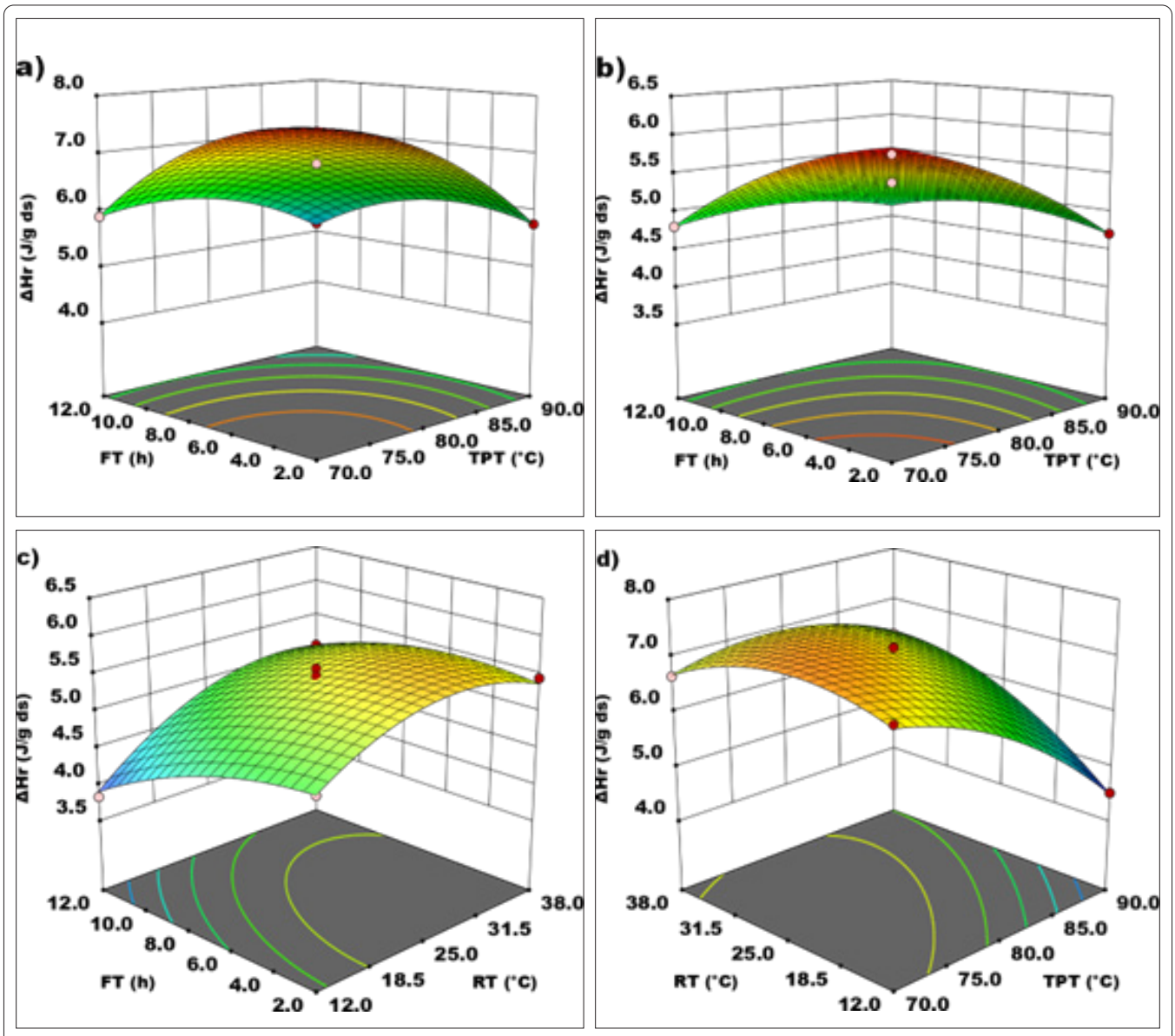

Figure 5: Quadratic response surfaces showing the combined effects of TPT, RT, and FT on the ΔH_r of UBF. **(a, d)** Correspond to *L. plantarum*, and **(b, c)** to *L. brevis*.

scission that shorten polymer chain as well as gradually erode both amorphous regions and previously retrograded domains [52]. Consequently, the fraction of ordered starch present as native and retrograded double helices decreases upon melting, while the enthalpic signal associated with these crystalline domains becomes weaker. In contrast, RT, with both a highly significant ($p < 0.0001$, table 4) positive linear (X_2) term and a negative quadratic (X_2^2) term, produced a complex concave response of ΔH_r. This pattern reflects a kinetically controlled process in which ΔH_r increases from low to intermediate RT, reaches a peak in the mid-range, and then declines to the highest RT. An intermediate RT offers an optimal balance between molecular mobility and available water, which allows chains to align and reorganize efficiently into stable crystallites [18, 43]. When RT is very low, chain mobility is strongly limited and the molecular alignment required for crystallization is hindered [44, 53]. At high RT, the thermodynamic driving force for crystallization diminishes as the temperature approaches the melting region of the retrograded phase [45, 50]. Under these conditions, higher thermal energy destabilizes newly formed crystallites and favors their partial dissolution. It leads to fewer or less perfect crystals and a lower final ΔH_r. This behavior confirms that RT mainly governs the kinetics and extent of recrystallization, whereas TPT and FT determine the quantity and structural quality of the crystallizable substrate. Moreover, the categorical factor representing the strain (X_4) also had a highly significant effect ($p < 0.0001$) on ΔH_r (Table 4). This result shows that the choice of microbial species controls the final recrystallization behavior of the starch substrate. The reduced cubic model yielded a negative CE for X_4 indicating that *L. brevis* consistently leads to lower ΔH_r values compared to *L. plantarum* under equivalent processing conditions. Besides, strong positive correlations were observed between ΔH_r and the RS fraction (Figure 3c and 3d). This trend shows that ΔH_r is an effective thermal proxy for the total amount of RS [47] formed during the sequential bioprocess. The strong negative correlations between ΔH_r and the PGI (Figure 3e and 3f) further show that greater crystalline struc-

ture, as reflected by ΔH_r, corresponds to a desirable reduction in starch digestibility and the resulting glycemic response [42, 54]. In addition, the reduced cubic model also showed that ΔH_r is strongly influenced by interaction effects (Table 4). Process outcome therefore depends on the combined action of the factors rather than on their individual contributions. The two-way interactions TPT × RT and TPT × FT were highly significant ($p < 0.0001$) and exhibited positive CE (Table 4). These positive interactions reveal that suitable combinations of cooling and fermentation conditions can partly counter the detrimental impact of intense thermal priming on ΔH_r. When TPT is high, an adequately chosen RT still promotes chain reorganization into ordered crystallites, and a controlled FT allows limited structural relaxation without excessive hydrolysis [31]. Otherwise, the compensatory effect weakens, and ΔH_r declines more sharply [44, 53]. Thus, although strong thermal priming lowers ΔH_r, the loss is less severe when it is followed by appropriate cooling or a moderated fermentation stage that enables partial chain realignment. On the other hand, the significant interaction between TPT and strain with a positive CE ($p < 0.001$, table 4), indicates that *L. brevis* is less affected by high TPT than *L. plantarum*. This can be ascribed to the milder biochemical environment promoted by *L. brevis*, which mitigates the impact of strong thermal priming on the crystalline fraction [49]. The significant X_3X_4 term with positive CE ($p < 0.001$) further shows that the decrease in ΔH_r with increasing FT is attenuated in *L. brevis*, consistent with its capacity to limit thermal disruption of crystalline structure through its milder biochemical environment [48, 55]. In addition, the significant quadratic linear terms $X_1^2X_4$ and $X_3^2X_4$ ($p < 0.05$, table 5) indicate that the strain modulates the curvature of ΔH_r with respect to TPT and FT. The positive CE of these terms reveals that in *L. brevis*, this curvature is reduced and ΔH_r changes more smoothly across the factor ranges. In contrast, *L. plantarum* is accentuated, with a narrow maximum and a steep decline at extreme priming temperatures and during prolonged fermentation. As depicted in figure 1d and 1e) the curves for *L. plantarum* remain above those for *L. brevis* across the ranges of TPT and FT, confirming higher ΔH_r for this species. The gap narrows at the highest TPT and with increasing FT, reflecting attenuation of thermal damage in the *L. brevis* system, which preserves and reorganizes disrupted starch chains [39], whereas *L. plantarum* degrades more rapidly retrograded helices [38]. The three-way interactions refine this picture further. The significant TPT × RT × strain term with negative CE ($p < 0.001$, table 4), indicates that the combination of high TPT and high RT is more destructive for ΔH_r in *L. plantarum* than in *L. brevis*. This means that when both heating and cooling are intense, the crystalline network in *L. plantarum* loses enthalpy more abruptly, whereas *L. brevis* favor ΔH_r retention. In addition, the RT ×FT × strain interaction shows a significant positive CE ($p < 0.05$, table 4), demonstrating that under prolonged fermentation, higher RT more effectively stabilizes ΔH_r in *L. brevis*. This highlights that the combined effect of appropriate cooling and controlled fermentation is particularly favorable for preserving the crystalline network in *L. brevis,* where lower depolymerizing activity reduces structural loss during extended processing [56]. These observations support the use of strain-specific quadratic models to describe ΔH_r behavior across different thermal and fermentation conditions.

The strain-specific models were significant ($p < 0.0001$ for *L. plantarum*; $p < 0.001$ for *L brevis*), with adjusted R^2 values above 0.969, coefficients of variation below 2.220 and non-significant lack of fit ($p > 0.05$), indicating strong model adequacy (Table 5 and table 6). In line with this, X_1X_3 has a positive CE in both *L. plantarum* and *L. brevis* ($p < 0.05$, table 5 and table 6), whereas X_2X_3 also exhibiting positive CE term and is significant only for *L. brevis* ($p < 0.05$, table 6). In *L. plantarum* X_1X_2 term is also significant ($p < 0.001$, table 5), which confirms the strong joint effect of TPT and RT on ΔH_r. This pattern is consistent with the trends observed in the three-way interactions. For *L. plantarum*, the response surfaces (Figure 5a and 5d) highlight the combined action of TPT with RT and FT. In figure 5a, ΔH_r shows a dome-shaped profile with a maximum at intermediate TPT and intermediate FT. Beyond this region, higher TPT or longer FT causes a sharp decline in ΔH_r, reflecting extensive gelatinization followed by acid- and amylase-driven degradation of retrograded crystallites [44, 56]. In figure 5d, intermediate RT partly offset the decrease. At low FT, ΔH_r is highest at mid-range RT and declines at lower or higher values. As a result, *L. plantarum* needs precise alignment of priming intensity, cooling temperature and fermentation duration to preserve high ΔH_r. In contrast, *L. brevis* exhibits a more stable response because FT acts together with priming and cooling temperatures to shape ΔH_r. Although ΔH_r decreases as TPT and FT rise, the surface is flatter and displays a broad zone of moderate values (Figure 5b and 5c). Wide plateaus maintain high ΔH_r across many RT × FT combinations, with declines occurring only at very long FT or extreme cooling. This stability reflects slower acidification, weaker amylase activity, and EPS production, which limit chain scission and preserve retrograded crystallites [48, 55].

Impact on BR

The reduced cubic model showed that sequential bioprocessing factors exerted a highly significant effect on BR ($p < 0.0001$, table 4), revealing that variations in these process parameters meaningfully altered the extent of structural degradation. At the main-effects level, both TPT (X_1) and FT (X_3) exhibited positive CE indicating that BR increases consistently as both TPT and FT rise. This trend aligns with the progressive structural degradation of the starch matrix, where high TPT induces extensive gelatinization and disrupts native RS2 granules [51]. In contrast, prolonged FT promotes acid and amylase-driven hydrolysis, which further weakens the starch network and reduces its capacity to withstand shear stress [15, 52]. These observations follow the principle that a loss of structural integrity, reflected by high BR, is closely linked to a reduction in nutritionally desirable RS [57]. This relationship is supported by the strong inverse correlation between BR and RS (Figure 3g and 3h) and by the high positive correlation with the PGI (Figure 3i and 3j). Conversely, RT (X_2) have a negative CE, signifying that BR decreases as RT increases towards intermediate values. Such a trend is indicative of enhanced retrogradation with RS3 formation, which strengthens the paste through the reassociation of starch chains into stable, shear-resistant crystallites [31, 43]. Evi-

dence of this mechanism is supported by the strong negative correlation observed between BR and the ΔH_r (Figure 3k and 3l), where the highest degree of starch recrystallization (high ΔH_r) corresponds to the lowest loss of paste stability (low BR). The non-linear behavior of BR was further confirmed by the highly significant ($p < 0.0001$) quadratic terms for X_2^1 and X_2^2, indicating that the structural changes influencing paste stability are not directly proportional to these factors. Furthermore, the LAB strain (X_4) had a highly significant effect on BR ($p < 0.0001$, table 4), with the positive CE indicating that *L. brevis* fermentation leads to higher BR compared to *L. plantarum*. This effect corresponds with the inverse relationship observed with RS and PGI for the *L. brevis* treatment. The high BR is likely due to the unique microenvironment generated by *L. brevis*, characterized by EPS production, that increases local viscosity and water binding [58]. Although the EPS matrix may protect against hydrolysis, it can sterically hinder the optimal alignment of starch chains required for forming a highly cohesive and shear-resistant gel [48]. As a result, BR remains high despite the potential for greater RS formation and lower PGI. In line with this strain effect, the quadratic linear $X_2^2X_4$ term was also significant ($p < 0.05$, table 4), indicating that the curvature of BR with respect to RT differs between the two LAB species and that the optimal cooling range for controlling breakdown is strain dependent. The sequential processing steps were also interdependent, as shown by the significant two-way interaction terms of the reduced cubic model. The TPT × RT interaction was the most significant ($p < 0.0001$) and had the largest negative CE. This demonstrates that an appropriate RT can partially offset the structural stability loss caused by intense thermal priming [18, 53]. This further highlights the importance of an optimal cooling step following gelatinization. Both X_1X_3 and X_2X_3 terms were significant ($p < 0.05$) and had negative CE. These results indicate that the benefits of TPT-induced solubilization and RT-induced strengthening are reduced when the starch matrix is exposed to prolonged acid and amylase hydrolysis during fermentation [15, 52]. Specifically, the negative X_2X_3 term shows that the stability advantage gained from optimal retrogradation is compromised by extended FT.

Strain-specific models for *L. plantarum* and *L. brevis* further confirmed the role of the LAB species in influencing BR. Both models were highly significant ($p < 0.001$, table 5 and table 6) and demonstrated strong adequacy, with adjusted R^2 values above 0.967, coefficients of variation below 0.663, and a non-significant lack of fit ($p > 0.05$). In both strains, X_1X_2 interaction term was significant ($p < 0.05$, table 5 and table 6), while the X_1X_3 interaction was significant for *L. brevis* ($p < 0.05$, table 6). Consistent with these interaction effects, the BR response surfaces as a function of TPT and RT were parabolic for both strains (Figure 6a and 6b), with the lowest BR values located in the central region of the design space at moderate TPT combined with intermediate RT. This pattern indicates that sufficient starch chain liberation by moderate thermal priming, followed by efficient recrystallisation during cooling, is required to minimize paste breakdown. Under these conditions, retrograded networks can form and stabilize the paste structure against shear induced disruption [18]. At very low TPT, granule disruption is limited and the matrix remains poorly retrogradable [44], whereas at the upper TPT range gelatinization becomes extensive and the matrix progressively loses strength [59]. Moving RT away from the intermediate range on either side also increases BR, because very low or very high RT restricts chain mobility and hinders effective starch reassociation [50, 53]. The quadratic strain-specific models also depict that the set of conditions associated with low BR depends on the LAB species. The response surface for *L. brevis* (Figure 6b) exhibits a broader minimum zone than that for *L. plantarum* (Figure 6a), consistent with the milder impact of *L. brevis* on acidification and enzymatic degradation. In the *L. brevis* model, the X_2X_3 interaction term was significant and exhibited negative CE ($p < 0.05$, table 6). The corresponding response surface (Figure 6c) slopes downward as both RT and FT increase, indicating that higher RT enhances the BR reducing effect of prolonged fermentation. High RT combined with prolonged FT therefore yields the lowest BR, suggesting enhanced starch chain reassociation during retrogradation under the protective biochemical environment created by *L. brevis* [58]. These outcomes highlight the complementary role of retrogradation and the protective effect of *L. brevis*. Together with the strong associations among BR, RS, PGI, and ΔH_r (Figure 3), these findings position BR as a sensitive indicator of overall structural integrity. They also show that paste stability is directly connected to nutritional quality through RS and PGI, and to physicochemical organization as reflected by ΔH_r.

Optimization of sequential bioprocessing factors

The optimal conditions for sequential bioprocessing were determined by simultaneous optimization of nutritional and techno-functional responses. The aim was to maximize RS and ΔH_r, while minimizing PGI and BR, with TPT, RT, and FT constrained within the experimental ranges. The multi response optimization identified distinct but closely related optima for the two LAB species (Table 7). The quadratic model predicted an optimum for *L. plantarum* at a TPT of 70 °C, RT of 26.92 °C and FT of 2.00 h. For *L. brevis*, the predicted optimum was slightly shifted, with a TPT of 70.90 °C, an RT of 24.60 °C and an FT of 2.05 h. In both cases, practical validation was performed under conditions slightly adjusted to suit pilot scale, namely TPT of 70 °C, RT of 25 °C and FT of 2 h. The experimental values obtained at these conditions agreed well with the predictions. Differences between predicted and measured responses were non-significant ($p > 0.05$) and remained within the experimental standard deviations. These experimental values were also confirmed to lie within the model 95% confidence intervals, which supports the accuracy and reliability of the models for predicting the optimized sequential bioprocessing conditions [60]. Under the optimal conditions for *L. plantarum*, RS, PGI, ΔH_r, and BR were all very close to their predicted values (Table 7). This outcome shows that moderate thermal priming, cooling in the mid-range and short fermentation act together to give a coherent profile. The UBF combines high RS, a well-developed retrograded structure, limited paste breakdown and a moderate glycemic response. This pattern is consistent with the factor effects discussed earlier, where intermediate RT and short FT stabilized the starch matrix and maintained low BR while preserving RS rich domains. In the other hand, the model val-

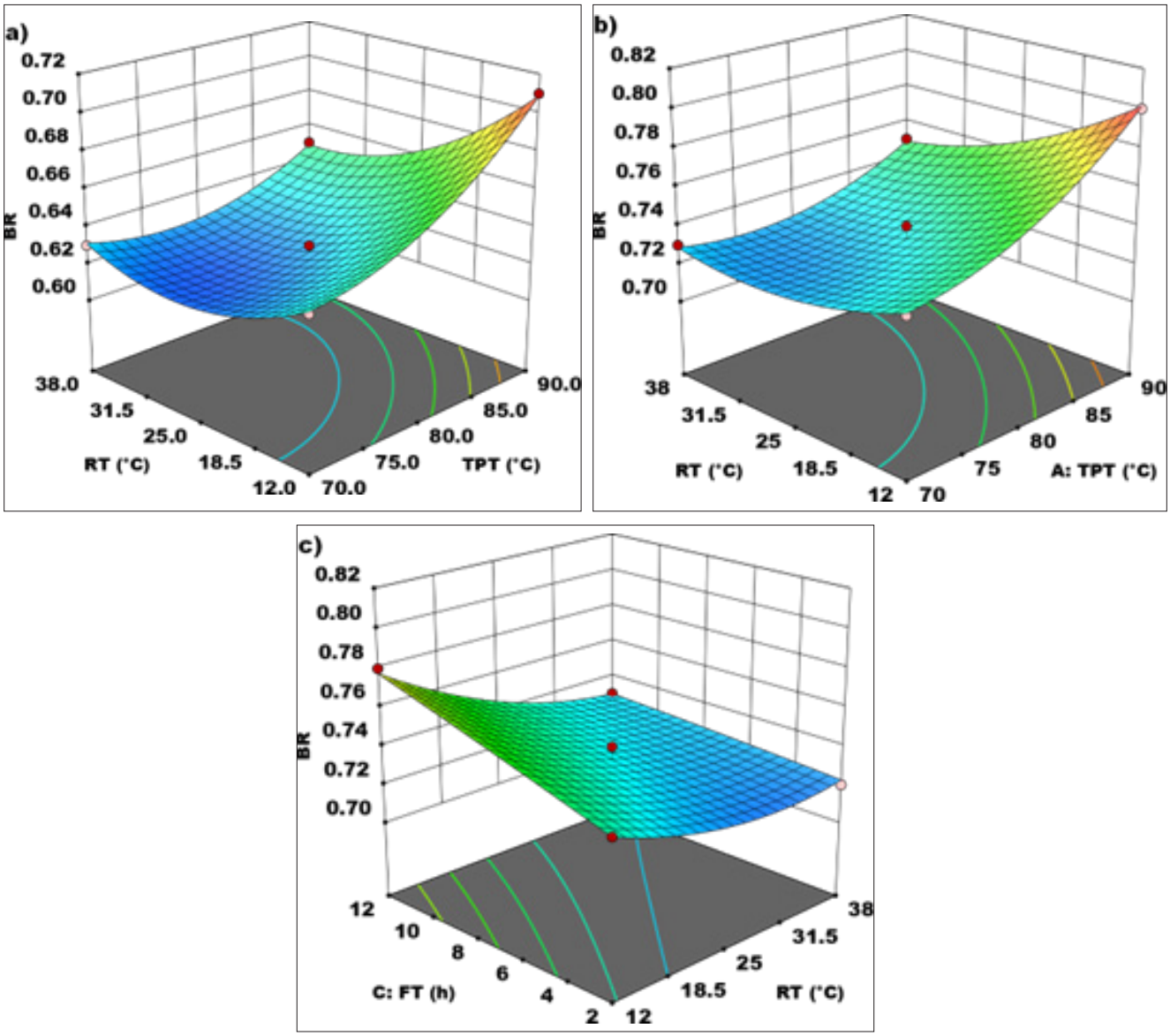

Figure 6: Quadratic response surfaces showing the combined effects of TPT, RT, and FT on the BR of UBF. **(a)** Correspond to *L. plantarum*, and **(b, c)** to *L. brevis*.

idation for *L. brevis* led to similar level of agreement between predicted and experimental values (Table 7). Compared with *L. plantarum* at its optimum, *L. brevis* gave higher RS and a slightly lower PGI, but lower ΔH_r and higher BR. This confirms the trade-off already observed in the response surfaces. *L. brevis* promotes RS accumulation and a lower glycemic response, but the retrograded network is less consolidated, and the paste is more prone to breakdown under shear. The comparison of the two species at their respective optima therefore reveals complementary behaviors. *L. plantarum* gives a stronger retrograded structure and lower BR, at the cost of slightly lower RS and a slightly higher PGI. In contrast, *L. brevis* maximizes RS and minimizes PGI, but yields a less resistant paste, as indicated by lower ΔH_r and higher BR. These differences are coherent with the strain specific patterns described for each response and with the stronger dependence of BR on the biochemical environment created by *L. brevis*. Overall, the optimization shows that a narrow window around TPT 70 °C, RT close to 25 °C and FT of about 2 h provides a robust compromise for sequential bioprocessing of UBF. Within this range, the choice of strain shifts the balance between structural consolidation and nutritional enhancement. The close agreement between predicted and experimental data supports the use of the models to guide process design and scale up and indicates that the selected conditions can be used to produce RS enriched, low PGI banana-based ingredients.

At the validated optimal conditions, the two species showed distinct but significative ($p < 0.05$, table 7) differences in performance. From a nutritional perspective, *L. brevis* provided the best profile yielding about 44.79% more RS than *L. plantarum* and lowering PGI by almost 4.74 units, which corresponds to roughly 8.76% on the PGI scale. This reduction is expected to lessen postprandial glucose peaks and may help moderate blood sugar responses. It can therefore contribute to better overall glycemic control when the UBF is incorporated into the diet, particularly in populations at risk for type 2 diabetes or metabolic syndrome. In contrast, *L. plantarum* exhibited superior techno-functional properties, with about 24.34%

Table 7: Predicted and experimental optimal conditions for LAB fermentation of unripe banana powder.

Variable	Goal	*L. plantarum*		*L. brevis*	
		Predicted values	Experimental values	Predicted values	Experimental values
Fermentation conditions					
TPT (˚C)	In range	70.00	70.00	70.90	70
RT (˚C)	In range	26.92	25.00	24.60	25
FT (h)	In range	2.00	2.00	2.05	2
Nutritional properties					
RS (g/100 g ds)	Maximize	12.80	12.39 ± 0.02[b]	17.55	17.94 ± 0.03[a]
PGI	Minimize	53.80	54.13 ± 0.08[a]	49.47	49.39 ± 0.06[b]
Techno-functional properties					
ΔH_r (J/g ds)	Maximize	7.79	7.56 ± 0.02[a]	6.12	6.08 ± 0.05[b]
BR	Minimize	0.61	0.59 ± 0.01[b]	0.71	0.72 ± 0.01[a]

Note: Mean percentages with different letters in the same column are significantly different at $p < 0.05$ (ANOVA, Tukey's test).

higher ΔH_r and approximately 18.06% lower BR. These differences indicate a more consolidated retrograded structure and a paste that is less prone to breakdown under shear. In practical terms, this behavior can improve paste stability during mixing, extrusion and cooking. It can also reduce defects such as syneresis or texture collapse, and enhance the structural integrity and cohesiveness of doughs, batters or cereal matrices. As a result, products formulated with plantarum fermented UBF are more robust during industrial processing and storage, while displaying more consistent product quality. Overall, the strain effect therefore acts as a fine-tuning lever. *L. brevis* shifts the profile toward nutritional enhancement, whereas *L. plantarum* favors paste stability and structural consolidation.

Conclusion

This study demonstrated that response surface methodology can effectively guide the optimization of sequential bioprocessing for UBF by capturing the coupled effects of thermal priming, retrogradation, and fermentation on both nutritional and techno functional attributes. The reduced cubic and strain specific quadratic models described the key responses with good adequacy, confirming that process performance is governed by interactions among the unit operations rather than by single factor effects. Pilot scale validation supported the predictive reliability of the models, indicating that the optimized conditions can be translated into practical process design. A consistent strain dependent pattern was observed at the optimized conditions. *L. brevis* favored nutritional improvement, whereas *L. plantarum* strengthened structural organization and paste stability. This confirms that LAB selection is a practical control point for tailoring the balance between glycemic related properties and processing robustness, depending on the target product. Overall, the findings establish a validated, process-based framework for producing functional UBF intended for cereal type applications. Future research should evaluate these optimized flours in real food matrices, investigate consumer acceptance, and assess their glycemic impact *in vivo* to confirm their commercial relevance.

Acknowledgements

None.

Conflict of Interest

None.

References

1. NCD Risk Factor Collaboration. 2024. Worldwide trends in diabetes prevalence and treatment from 1990 to 2022: a pooled analysis of 1108 population-representative studies with 141 million participants. *Lancet* 404(10467): 2077-2093. https://doi.org/10.1016/s0140-6736(24)02317-1
2. Silva-Paz RJ, Silva-Lizárraga RR, Jamanca-Gonzales NC, Eccoña-Sota A. 2024. Evaluation of the physicochemical and sensory characteristics of gluten-free cookies. *Front Nutr* 10: 1-8. https://doi.org/10.3389/fnut.2023.1304117
3. Dega V, Barbhai MD. 2023. Exploring the underutilized novel foods and starches for formulation of low glycemic therapeutic foods: a review. *Front Nutr* 10: 1-16. https://doi.org/10.3389/fnut.2023.1162462
4. Maseko KH, Regnier T, Meiring B, Wokadala OC, Anyasi TA. 2024. Musa species variation, production, and the application of its processed flour: a review. *Sci Hortic* 325: 112688. https://doi.org/10.1016/j.scienta.2023.112688
5. Suo X, Baggio A, Pellegrini N, Vincenzetti S, Vittadini E. 2024. Effect of shape, gluten, and mastication effort on *in vitro* starch digestion and the predicted glycemic index of pasta. *Food Funct* 15(1): 419-426. https://doi.org/10.1039/d3fo02666c
6. Culetu A, Duta DE, Papageorgiou M, Varzakas T. 2021. The role of hydrocolloids in gluten-free bread and pasta; rheology, characteristics, staling and glycemic index. *Foods* 10(12): 3121. https://doi.org/10.3390/foods10123121
7. García-Vázquez C, Ble-Castillo JL, Arias-Córdova Y, Ramos-García M, Olvera-Hernández V, et al. 2023. Effects of resistant starch on glycemic response, postprandial lipemia and appetite in subjects with type 2 diabetes. *Eur J Nutr* 62(5): 2269-2278. https://doi.org/10.1007/s00394-023-03154-4
8. Medina MDR, Ruales J. 2024. Post-harvest alternatives in banana cultivation. *Agronomy* 14(9): 2109. https://doi.org/10.3390/agronomy14092109
9. Krungkaew S, Hülsemann B, Kingphadung K, Mahayothee B, Oechsner H, et al. 2023. New sustainable banana value chain: waste valuation toward a circular bioeconomy. *Energies* 16(8): 3453. https://doi.org/10.3390/en16083453
10. Ntabo AN, Okello DO, Muange EN. 2024. Determinants of utilization of banana value addition among small-scale agripreneurs in Kenya: a case of Kisii County. *J Dev Agric Econ* 16(1): 1-14. https://doi.org/10.5897/jdae2023.1398

11. Dibakoane SR, Du Plessis B, Da Silva LS, Anyasi TA, Emmambux MN, et al. 2023. Nutraceutical properties of unripe banana flour resistant starch: a review. *Starch* 75(9-10): 2200041. https://doi.org/10.1002/star.202200041
12. Cheng Y, Huang P, Chan Y, Chiang P, Lu W, et al. 2024. Investigate the composition and physicochemical properties attributes of banana starch and flour during ripening. *Carbohydr Polym Technol Appl* 7: 100446. https://doi.org/10.1016/j.carpta.2024.100446
13. Biernacka B, Dziki D, Różyło R, Gawlik-Dziki U. 2020. Banana powder as an additive to common wheat pasta. *Foods* 9(1): 53. https://doi.org/10.3390/foods9010053
14. Sabater C, Sáez GD, Suárez N, Garro MS, Margolles A, et al. 2024. Fermentation with lactic acid bacteria for bean flour improvement: experimental study and molecular modeling as complementary tools. *Foods* 13(13): 2105. https://doi.org/10.3390/foods13132105
15. Wei C, Ge Y, Zhao S, Liu D, Jiliu J, et al. 2022. Effect of fermentation time on molecular structure and physicochemical properties of corn ballast starch. *Front Nutr* 9: 1-12. https://doi.org/10.3389/fnut.2022.885662
16. Baptista NT, Dessalles R, Illner A-K, Ville P, Ribet L, et al. 2024. Harnessing the power of resistant starch: a narrative review of its health impact and processing challenges. *Front Nutr* 11: 1-12. https://doi.org/10.3389/fnut.2024.1369950
17. Huang S, Chao C, Yu J, Copeland L, Wang S. 2021. New insight into starch retrogradation: the effect of short-range molecular order in gelatinized starch. *Food Hydrocoll* 120: 106921. https://doi.org/10.1016/j.foodhyd.2021.106921
18. Li C. 2024. Unraveling the complexities of starch retrogradation: insights from kinetics, molecular interactions, and influences of food ingredients. *Food Rev Int* 40(9): 3159-3182. https://doi.org/10.1080/87559129.2024.2347467
19. Ma Z, Hu X, Boye JI. 2020. Research advances on the formation mechanism of resistant starch type III: a review. *Crit Rev Food Sci Nutr* 60(2): 276-297. https://doi.org/10.1080/10408398.2018.1523785
20. Du L, Jaya Prasad A, Gänzle M, Roopesh MS. 2020. Inactivation of *Salmonella* spp. in wheat flour by 395 nm pulsed light emitting diode (LED) treatment and the related functional and structural changes of gluten. *Food Res Int* 127: 108716. https://doi.org/10.1016/j.foodres.2019.108716
21. Kwaw E, Ma Y, Tchabo W, Apaliya MT, Wu M, et al. 2018. Effect of lactobacillus strains on phenolic profile, color attributes and antioxidant activities of lactic-acid-fermented mulberry juice. *Food Chem* 250: 148-154. https://doi.org/10.1016/j.foodchem.2018.01.009
22. Khoozani AA, Bekhit AE-DA, Birch J. 2019. Effects of different drying conditions on the starch content, thermal properties and some of the physicochemical parameters of whole green banana flour. *Int J Biol Macromol* 130: 938-946. https://doi.org/10.1016/j.ijbiomac.2019.03.010
23. Giuberti G, Gallo A, Cerioli C, Masoero F. 2012. *In vitro* starch digestion and predicted glycemic index of cereal grains commonly utilized in pig nutrition. *Anim Feed Sci Technol* 174(3): 163-173. https://doi.org/10.1016/j.anifeedsci.2012.03.006
24. Dong R, Niu Q, Zhang K, Hu X, Bu Y. 2020. The effect of retrogradation time and ambient relative humidity on the quality of extruded oat noodles. *Food Sci Nutr* 8(6): 2940-2949. https://doi.org/10.1002/fsn3.1596
25. Kongolo JI, Da Silva LS, Wokadala OC, Du Plessis B, Husselman J, et al. 2017. Pasting, thermal, gel texture, resistant starch and colour properties of unripe banana flour from 10 desert banana varieties cultivated in South Africa. *J Food Meas Charact* 11(3): 1056-1064. https://doi.org/10.1007/s11694-017-9481-x
26. Tchabo W, Ma Y, Kwaw E, Zhang H, Li X. 2017. Influence of fermentation parameters on phytochemical profile and volatile properties of mulberry (*Morus nigra*) wine. *J Inst Brew* 123(1): 151-158. https://doi.org/10.1002/jib.401
27. Tchabo W, Ma Y, Engmann FN, Zhang H. 2015. Ultrasound-assisted enzymatic extraction (UAEE) of phytochemical compounds from mulberry (*Morus nigra*) must and optimization study using response surface methodology. *Ind Crops Prod* 63: 214-225. https://doi.org/10.1016/j.indcrop.2014.09.053
28. Liu S, Reimer M, Ai Y. 2020. *In vitro* digestibility of different types of resistant starches under high-temperature cooking conditions. *Food Hydrocoll* 107: 105927. https://doi.org/10.1016/j.foodhyd.2020.105927
29. Liu X, Huang S, Chao C, Yu J, Copeland L, et al. 2022. Changes of starch during thermal processing of foods: current status and future directions. *Trends Food Sci Technol* 119: 320-337. https://doi.org/10.1016/j.tifs.2021.12.011
30. Górecki AR, Blaszczak W, Lewandowicz J, Le Thanh-Blicharz J, Penkacik K. 2018. Influence of high pressure or autoclaving-cooling cycles and pullulanase treatment on buckwheat starch properties and resistant starch formation. *Pol J Food Nutr Sci* 68(3): 235-242. https://doi.org/10.1515/pjfns-2018-0001
31. Soler A, Velazquez G, Velazquez-Castillo R, Morales-Sanchez E, Osorio-Diaz P, et al. 2020. Retrogradation of autoclaved corn starches: effect of water content on the resistant starch formation and structure. *Carbohydr Res* 497: 108137. https://doi.org/10.1016/j.carres.2020.108137
32. Abedi E, Sayadi M, Oliyaei N, Zhang P. 2025. The underlying mechanism of resistant starch production through esterification a substitution or crosslinking by citric, malic, and lactic acid after freezing pre-treatment: comparative study on production efficiency, digestibility, pasting, and thermal properties. *Food Chem* 476: 143441. https://doi.org/10.1016/j.foodchem.2025.143441
33. Aaliya B, Sunooj KV. 2021. Influence of organic acids on a non-conventional starch from *Corypha umbraculifera* L. to improve its functionality and resistant starch content. *Biol Life Sci Forum* 6(1): 4. https://doi.org/10.3390/foods2021-11001
34. Klostermann CE, Buwalda PL, Leemhuis H, de Vos P, Schols HA, et al. 2021. Digestibility of resistant starch type 3 is affected by crystal type, molecular weight and molecular weight distribution. *Carbohydr Polym* 265: 118069. https://doi.org/10.1016/j.carbpol.2021.118069
35. Afreen A, Ahmed Z, Khalid N. 2023. Optimization, fractional characterization, and antioxidant potential of exopolysaccharides from *Levilactobacillus brevis* NCCP 963 isolated from kanji. *RSC Adv* 13(29): 19725-19737. https://doi.org/10.1039/d2ra07338b
36. Eze CO, Berebon DP, Gugu TH, Anazodo FI, Okorie JE. 2022. Lactobacillus Exopolysaccharide: An Untapped Biopolymer. In Laranjo M (ed) Lactobacillus – A Multifunctional Genus. IntechOpen, London.
37. Wang Y, Wu J, Lv M, Shao Z, Hungwe M, et al. 2021. Metabolism characteristics of lactic acid bacteria and the expanding applications in food industry. *Front Bioeng Biotechnol* 9: 1-19. https://doi.org/10.3389/fbioe.2021.612285
38. Zhang J, Liu Y, Liu M, Zhao Y, Zhu Y, et al. 2024. Effects of *Lactiplantibacillus plantarum* dy-1 fermentation on multi-scale structure and physicochemical properties of barley starch. *Food Funct* 15(4): 1923-1937. https://doi.org/10.1039/d3fo04395a
39. Alkay Z, Alkay R, Dertli E, Kökten K, Durak M. 2023. Rheological, textural and physicochemical properties of buckwheat sourdough bread prepared with different lactic acid bacteria strains. *J Microbiol Biotechnol Food Sci* 12(5): 1-5. https://doi.org/10.55251/jmbfs.5643
40. Di Biase M, Le Marc Y, Bavaro AR, Lonigro SL, Verni M, et al. 2022. Modeling of growth and organic acid kinetics and evolution of the protein profile and amino acid content during *Lactiplantibacillus plantarum* ITM21B fermentation in liquid sourdough. *Foods* 11(23): 3942. https://doi.org/10.3390/foods11233942
41. Lin W, Zhang D, Huang J, Lei Y, Su X, et al. 2024. Expression and characterization of a maltogenic amylase from *Lactobacillus plantarum* in *Escherichia coli* and its application in extending bread shelf life. *Syst Microbiol Biomanuf* 4(1): 318-327. https://doi.org/10.1007/s43393-022-00155-y

42. Cesbron-Lavau G, Goux A, Atkinson F, Meynier A, Vinoy S. 2021. Deep dive into the effects of food processing on limiting starch digestibility and lowering the glycemic response. *Nutrients* 13(2): 381. https://doi.org/10.3390/nu13020381

43. Ding L, Yang J, Kirkensgaard JJK, Enemark-Rasmussen K, Chang J, et al. 2025. Characterization of different high amylose starch granules. Part III: how starch fine structures affect retrogradation and formation of type 3 resistant starch. *Carbohydr Polym* 361: 123633. https://doi.org/10.1016/j.carbpol.2025.123633

44. Chakraborty I, Govindaraju I, Kunnel S, Managuli V, Mazumder N. 2023. Effect of storage time and temperature on digestibility, thermal, and rheological properties of retrograded rice. *Gels* 9(2): 142. https://doi.org/10.3390/gels9020142

45. Li M, Zhang H, Lyu L, Deng Q, Fan H, et al. 2024. Effects of sourdough on bread staling rate: from the perspective of starch retrogradation and gluten depolymerization. *Food Biosci* 59: 103877. https://doi.org/10.1016/j.fbio.2024.103877

46. Nguyen PT, Nguyen TT, Bui DC, Hong PT, Hoang QK, et al. 2020. Exopolysaccharide production by lactic acid bacteria: the manipulation of environmental stresses for industrial applications. *AIMS Microbiol* 6(4): 451-469. https://doi.org/10.3934/microbiol.2020027

47. Feng H, Cheng B, Lim J, Li B, Li C, et al. 2024. Advancements in enhancing resistant starch type 3 (RS3) content in starchy food and its impact on gut microbiota: a review. *Compr Rev Food Sci Food Saf* 23(3): e13355. https://doi.org/10.1111/1541-4337.13355

48. Buksa K, Kowalczyk M, Boreczek J. 2021. Extraction, purification and characterisation of exopolysaccharides produced by newly isolated lactic acid bacteria strains and the examination of their influence on resistant starch formation. *Food Chem* 362: 130221. https://doi.org/10.1016/j.foodchem.2021.130221

49. Demirkesen-Bicak H, Arici M, Yaman M, Karasu S, Sagdic O. 2021. Effect of different fermentation condition on estimated glycemic index, *in vitro* starch digestibility, and textural and sensory properties of sourdough bread. *Foods* 10(3): 514. https://doi.org/10.3390/foods10030514

50. Wang S, Zhang X, Wang S, Copeland L. 2016. Changes of multi-scale structure during mimicked DSC heating reveal the nature of starch gelatinization. *Sci Rep* 6(1): 1-9. https://doi.org/10.1038/srep28271

51. Wang S, Copeland L. 2013. Molecular disassembly of starch granules during gelatinization and its effect on starch digestibility: a review. *Food Funct* 4(11): 1564-1580. https://doi.org/10.1039/c3fo60258c

52. Li H, Zhu Y, Jiao A, Zhao J, Chen X, et al. 2013. Impact of α-amylase combined with hydrochloric acid hydrolysis on structure and digestion of waxy rice starch. *Int J Biol Macromol* 55: 276-281. https://doi.org/10.1016/j.ijbiomac.2013.01.021

53. Li C, Hamaker BR. 2021. Effects of different storage temperatures on the intra- and intermolecular retrogradation and digestibility of sago starch. *Int J Biol Macromol* 182: 65-71. https://doi.org/10.1016/j.ijbiomac.2021.03.195

54. Lal MK, Singh B, Sharma S, Singh MP, Kumar A. 2021. Glycemic index of starchy crops and factors affecting its digestibility: a review. *Trends Food Sci Technol* 111: 741-755. https://doi.org/10.1016/j.tifs.2021.02.067

55. Kwun S-Y, Yoon J-A, Kim G-Y, Bae Y-W, Park E-H, et al. 2024. Isolation of a potential probiotic *Levilactobacillus brevis* and evaluation of its exopolysaccharide for antioxidant and α-glucosidase inhibitory activities. *J Microbiol Biotechnol* 34(1): 167-175. https://doi.org/10.4014/jmb.2304.04043

56. Li H, Gilbert RG, Gidley MJ. 2021. Molecular-structure evolution during *in vitro* fermentation of granular high-amylose wheat starch is different to *in vitro* digestion. *Food Chem* 362: 130188. https://doi.org/10.1016/j.foodchem.2021.130188

57. Santamaria M, Montes L, Garzon R, Moreira R, Rosell CM. 2022. Unraveling the impact of viscosity and starch type on the *in vitro* starch digestibility of different gels. *Food Funct* 13(14): 7582-7590. https://doi.org/10.1039/d2fo00697a

58. Korcz E, Varga L. 2021. Exopolysaccharides from lactic acid bacteria: techno-functional application in the food industry. *Trends Food Sci Technol* 110: 375-384. https://doi.org/10.1016/j.tifs.2021.02.014

59. Mauro RR, Vela AJ, Ronda F. 2023. Impact of starch concentration on the pasting and rheological properties of gluten-free gels. Effects of amylose content and thermal and hydration properties. *Foods* 12(12): 2281. https://doi.org/10.3390/foods12122281

60. Tchabo W, Ma Y, Kaptso GK, Kwaw E, Cheno RW, et al. 2019. Process analysis of mulberry (*Morus alba*) leaf extract encapsulation: effects of spray drying conditions on bioactive encapsulated powder quality. *Food Bioprocess Technol* 12(1): 122-146. https://doi.org/10.1007/s11947-018-2194-2